Granular Matter (2016) 18:67
DOI 10.1007/s10035-016-0659-4

ORIGINAL PAPER

Unexpected liquefaction under isotropic consolidation of idealized granular materials

T. Doanh[1] · N. Abdelmoula[1] · T. T. T. Nguyen[1] · S. Hans[1] · C. Boutin[1] · A. Le Bot[2]

Received: 21 August 2015

Abstract The drained isotropic compression behaviour of very loose and fully saturated monodisperse glass beads in triaxial compression is investigated in this paper. Short cylindrical samples were prepared by moist-tamping technique and isotropically compressed in a classical axisymmetric triaxial machine. Very loose glass bead samples exhibit numerous local collapses with sudden volumetric compaction and axial contraction of very large amplitude and experience ultimately global collapse with spontaneous liquefaction under undetermined external isotropic stress. Excess pore pressure instantaneously generated at the beginning of the collapse phenomenon, and rapidly dissipated with the usual drainage system, shows a global complex system with local dynamic instability. The dynamic time evolution of the excess pore pressure ΔU consists in a first and fast transient phase *I* at constant volume and constant axial strain with large spikes ΔU^{peak}, followed by an intermediate second phase *II* of large increase of volumetric compaction and axial contraction at stabilizing ΔU_{stable} or constant effective stress σ' and finally a third and longest phase *III* of excess pore water pressure dissipation at nearly constant axial strain toward the initial back-pressure. For local collapses, the second phase is totally missing. Upon ignoring the local collapses, very loose idealized granular materials have a unique and global isotropic compressibility behaviour, independently of the void ratio at the end of the fabrication stage; and liquefaction-free for dense state below a threshold void ratio at fabrication e_{30}^{liq}, representing the transition from global instability with total failure to local instability with partial collapse. This paper provides the first reported spontaneous liquefaction instability under isotropic consolidation. It gives the necessarily conditions for an isotropic liquefaction and emphases some usually hidden or partially developed mechanisms underlying the diffuse instability phenomenon and adds a new intriguing layer to the complex behaviour of idealized granular materials in classical drained triaxial isotropic compression.

Keywords Liquefaction · Diffuse instability · Idealized granular materials · Isotropic consolidation · Friction · Dynamic

1 Introduction

Soil liquefaction is an important component of the mechanical behaviour of granular materials. Once liquefied, the granular soils entirely lose their shear strength leading to devastating consequences such as catastrophic collapse of structures or dramatic landslides. Consequently, a large number of intensive theoretical and experimental studies has been devoted to the understanding of this particular phenomenon, since the early days of soil mechanics.

The conventional understanding of liquefaction relies heavily on three simple and powerful ideas. The first one concerns the effective stress concept for fully saturated soils. Following the Terzaghi principle [71], the effective stress is $\sigma' = \sigma - u$, where σ the total stress and u the pore pressure. The second idea is the simple Mohr-Coulomb linear law

Electronic supplementary material The online version of this article (doi:10.1007/s10035-016-0659-4) contains supplementary material, which is available to authorized users.

✉ T. Doanh
thiep.doanh@entpe.fr

[1] Ecole Nationale des Travaux Publics de l'Etat. LGCB, LTDS (UMR 5513), 2 Rue M. Audin, 69518 Vaulx en Velin Cedex, France

[2] Ecole Centrale de Lyon. LTDS (UMR 5513). 36 avenue Guy-de-Collongue, 69134 Ecully Cedex, France

Published online: 11 July 2016

of friction for cohesionless materials. The shear strength is $\tau = \sigma' \tan(\phi)$, where ϕ is the intergranular frictional angle. A vanishing effective stress state can be obtained when the pore pressure rises up to the total stress level, resulting in a null shear strength and consequently the failure of soil with large deformation. The soil then flows under a very small shear stress like a fluid characterising a liquefied state. The third core idea relates to the soil dilatancy, Schofield et al. [67]. Above a critical void ratio, the soil contracts while increasing the effective stress but dilates for denser samples below this critical void ratio.

Experiments with real soils have rapidly shown two ways to elevate the pore pressure for fully saturated soils in undrained shearing. Both are obtained by imposing an external shear stress either by monotonic or by cyclic loading. Under monotonic loading, the undrained condition prevents a volume variation which is compensated by an interstitial pore pressure increase. Under cyclic loading, an overall pore pressure increase is also obtained with an alternate change from volumetric compaction to volumetric dilation regimes.

The first approach using monotonic loading leads to static liquefaction, obtained mainly and uniquely for initially loose granular materials, and the second approach to cyclic or dynamic liquefaction for broader range of densities. In either case, the evolution of pore pressure is of paramount importance, and all testing equipments of soil mechanics were successively used to study this pore pressure evolution first for initially isotropic sands, due to the technical constraint, the early availability and the simplicity of triaxial equipment, and later on anisotropic materials to better simulate natural sands.

Because of the natural similarity with liquefaction induced by seismic waves during earthquakes, in the early days of soil mechanics cyclic liquefaction was first investigated in laboratories using conventional and dynamic triaxial machines by Seed et al. [68], Yoshimi et al. [84], Ishihara et al. [41–43], Vaid et al. [74], among others to identify the dependency of pore pressure on some relevant parameters such as the void ratio at the beginning of undrained shearing, the double-amplitude of axial strain in cyclic loading, leading to the definition of liquefaction potential. For practical use, its quantitative definition relies on numerous experimental correlations with field tests, especially the popular Standard Penetration Test or Cone Penetration Test [39,72]. Later on, more complex machines such as true triaxial, Lanier et al. [54], simple shear, De Alba et al. [15], hollow cylinder, Ishihara et al. [40] and plane strain machines, Masuda et al. [57], were solicited to investigate the additional effects of principal stress rotation, intermediate principal stress and induced anisotropy on the liquefaction potential. Even dense sands can liquefy under simple but repetitive loadings, demonstrating the importance and the complexity of the still elusive induced anisotropy and liquefaction phenomenon.

Monotonic shear loading received much less attention than cyclic loading in the exploration of liquefaction, excepting some pioneer works Castro [12], Casagrande [11]. Recently, it was progressively adopted in a slower pace using the same laboratory equipment to investigate the static full liquefaction with its dynamic instabilities at large strains on loose soils. It slowly becomes one of the most challenging building blocks for benchmarking constitutive models and helps to discover a whole new class of failure well inside the Mohr-Coulomb's criterion, therefore, changing for ever the landscape of granular modelling Daouadji et al. [14], Ramos et al. [66]. It is termed as diffuse or homogeneous failure, dictated by the negativeness of the second-work order and associated with deviatoric stress peak and partial liquefaction, Lade et al. [52], Konrad et al. [47], Doanh et al. [21], Gajo et al. [29], Vaid [74], Yamada et al. [82] for citing a few.

The particular cases of isotropic loading, monotonic or cyclic, are infrequently studied. However, the early works of Fragaszy and Voss [26] show a rare case of liquefaction of Eniwetok sand under the unloading part of a single isotropic undrained cycle of high pressures.

Liquefaction, in the current mainstream of soil mechanics, is always related to an important reduction of effective stress, due to a fast or progressive variation of the excess pore pressure. It mostly occurs under shear of loose and fully saturated granular materials in *undrained* or partially drained loading conditions. However, it requires an external shearing source to create an *anisotropic* stress state. On the contrary, in drained condition with an isotropic compression, only an isotropic strain state is possible. The fluid pore pressure being maintained constant by the drained condition, the effective stress can only increase [71]. Even an inherently or stress-induced anisotropic medium can only have a smooth anisotropic strain behaviour when isotropically or uniaxially compressed [4,10,56]. This is why an isotropic liquefaction is *a priori* not expected. However, this argument is not always valid; and we shall show situations in which liquefaction can happen in isotropic drained compression.

Liquefaction can be seen as a particular response of civil engineering materials under extreme conditions [8]. The liquefaction experiments bear some resemblances to those exposed to impulsive shear stress load (blast waves [38], impact [48]) or to avalanches, landslides and earthquakes [6]. However, can liquefaction occur at the low-end of the extreme loading conditions, i.e. moderate overpressure ($\leqslant$1 MPa), low stress rate ($\leqslant$1 kPa/s), low temperature (ambient) and *without any macroscopic shear stress*?

Despite the large body of accumulated experimental knowledge, the physical significance behind liquefaction is far from fully understood; although liquefaction, static or dynamic, may be described by numerous phenomenological constitutive models [45,53,58,63,70]. Until now, some basic questions remain unsatisfactorily answered: What are

the physical triggering mechanisms, leading to the buildup of pore pressure capable to annihilate the effective stress? What are the physical parameters controlling the pore pressure or the effective stress evolution? In others words, the main question is quite simple: What precisely causes liquefaction?

The purpose of this paper is to investigate the mechanical behaviour of ideal granular materials, particularly the liquefaction in triaxial *isotropic* compression in *drained* condition, without any external shearing component. It presents new unconventional experimental findings of a comprehensive programme on very loose and saturated monodisperse glass beads in classical triaxial machine with emphasis of static and dynamic measurements of axial strain, volumetric strain, cell and pore pressure. Only the effects of effective isotropic stress are considered in this paper. Glass bead samples were prepared by moist tamping technique and isotropically compressed with constant stress rate.

This paper provides the first full report of spontaneous liquefaction under isotropic consolidation, i.e. isotropic compression while keeping the pore fluid pressure constant, of model granular materials, beside the preliminary brief report [22]. More importantly, it emphases the possibility of examining some mechanisms underlying the diffuse instability phenomenon; these mechanisms, usually hidden or partially developed in real granular materials (i.e. sands) are greatly amplified with the use of model granular materials (i.e. glass beads).

The adopted structure of the paper is as follows. Sect. 2 describes the experimental programme including the idealized material and the sets of laboratory tests. The experimental data shows very strong structural instabilities, affecting the global effective stress-strain behaviour and even leads to unusual spontaneous liquefaction in isotropic consolidation. These remarkable instabilities and their dependence on the initial void ratio and triggered isotropic stress are reported in Sect. 3. Specific features of individual instability events, including the ultimate liquefaction event, are studied in Sec. 4, together with some possible driving physical mechanisms. Finally, the paper highlights the essential unclassical findings in the conclusion section.

2 Experimental programme

Industrial soda lime spherical glass beads "Sil-glass" were used in this experimental study. They were commercialized by CVP, Linselles, France.[1] The usual index properties are reported in Table 1. To obtain a unimodal grain size distribution, glass beads were first manually sieved to eliminate the small amount of beads smaller than 0.3 mm diameter. Figure 1 presents the grading curve using particle size analyzer

[1] www.Cvp-abrasif-broyage.com.

Table 1 Index properties of SLG 6–8 glass beads

Property	Value
Density, ρ (kg/m^3)	2500
Mean size, D_{50} (mm)	0.723
Uniformity coefficient, C_u	1.463
Curvature coefficient, C_c	0.989
Maximum void ratio, e_{max}	0.686
Minimum void ratio, e_{min}	0.574

performed by laser diffraction, the frequency histogram and the image of virgin perfectly spherical glass beads SLG 6-8 viewed under SEM (Scanning Electron Microscopy). The frequency histogram indicates a slightly asymmetric distribution, resulting in a nearly monodisperse system with less than 1 % of larger beads above 1.5 mm diameter, twice as big as the average diameter D_{50}. These glass beads have a static friction coefficient of 0.24, according to CVP. In United Soil Classification System, these nearly monodisperse glass beads can be classified as clean and poorly graded fine-grained granular media Sm(SP) with $D_{50} = 0.723$ mm, uniformity coefficient $C_u = D_{60}/D_{10} = 1.463$, curvature coefficient $C_c = D_{30}^2/D_{60}D_{10} = 0.989$; D_i is the diameter for which i % of grains have diameter less than D_i; C_u and C_c two simple shape parameters. They belong to the same USCS classification encompassing the reference Hostun or Toyoura sand in the geotechnical literature [25,75], although these sands are much finer. Consequently, the glass beads are often considered as idealized granular materials. A monodispersed population of regular and ideal grain shapes, i.e. spherical glass beads, cannot, evidently represent the real soil grains having irregular and angular shapes, however, it constitutes a very first useful laboratory step towards a better understanding of the latter.

Very loose granular samples at fabrication stage were prepared using a modified moist tamping and under compaction method, inspired by the early works of Bjerrum et al. [7] and Ladd [50] on sand. This method was routinely used in soil laboratory to create granular samples with large initial void ratios at fabrication stage, and to obtain a fully contractive behaviour in triaxial compression, approaching the critical state. Moist-tamped samples were prepared by placing predetermined quantities of moist glass beads, mixed with 2 % of distilled water in weight, and gently compacted in five layers of prescribed thickness using a flat-bottom circular stainless steel tamper of 20 mm in diameter. Special care was given to have samples with nearly identical void ratios at fabrication state to minimize the well-known effect of density on the observed behaviour. Short samples, 70 mm in height and 70 mm in diameter, were prepared with enlarged and lubricated end plates to produce homogeneous deformations at large strains during shear. Cylindrical and open-ended latex

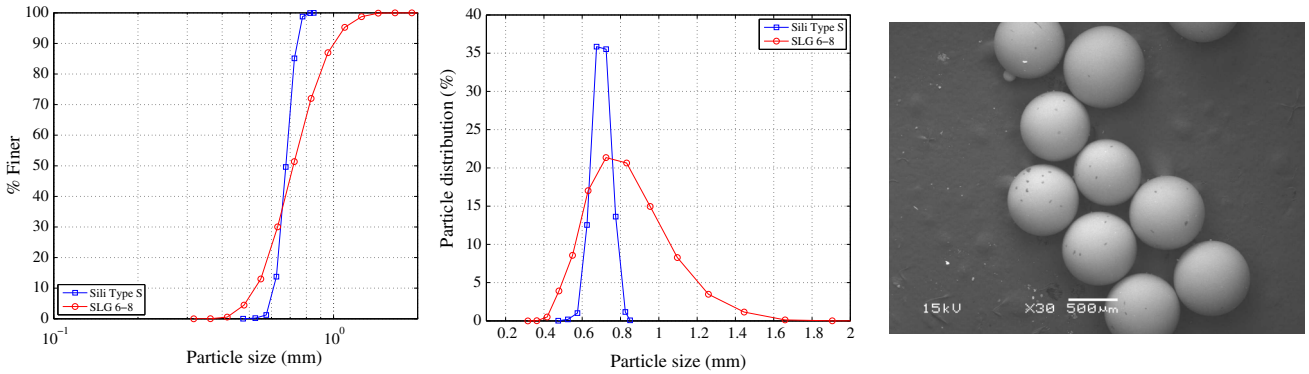

Fig. 1 Particle size distribution, frequency histogram and SEM image of SLG 6–8 glass beads of 0.7 mm of diameter

membrane of 0.3 mm of thickness were used. The elastic modulus of latex membrane was estimated at about only 2 MPa. CO_2 method [51] with de-aired distilled water, and back pressure of up to 200 kPa were applied to fully saturate granular samples to obtain Skempton's coefficient B higher than 0.95.

The void ratio (V_{void}/V_{grains}) of each granular sample was evaluated from the water content obtained at the end of the isotropic consolidation e_c or at the end of the subsequent undrained test. All glass beads and water were carefully retrieved in a duralumin tray and weighted with a tolerance of 0.1 g. e_c was determined after oven-drying and the void ratio e_{30} at the beginning of the isotropic consolidation at 30 kPa was deduced from volumetric measurement. As indicated by Verdugo and Ishihara [75], the void ratios estimated from water content at the end of the test are more accurate and reliable than those determined from the usual procedure of measuring sample dimensions. The void ratio e can be transformed to the volume fraction ($\Phi = V_{grains}/V_{total} = 1/(1+e)$), often used by physicists; or porosity ($\varepsilon = V_{void}/V_{total} = e/(1+e)$) used by porous-media scientists.

The experimental works were conducted using a modified classical triaxial system, Fig. 2. All tests were isotropically compressed in a manually stress-controlled mode with approximatively constant stress rate. The total isotropic stress σ was imposed using compressed air and the cell chamber was three-quarter filled with distilled water. To estimate the axial strain ε_a, the axial displacement was measured inside the triaxial cell by a linear variable differential transformer (LVDT) sensor mounted directly on the top platen. Another LVDT sensor converted the displacement of a membrane to the global volumetric strain ε_v from the water expelled from or moving into the sample. The pore-water pressure U was measured near the top cap of the granular sample, at a distance of about 60 cm, since the back pressure U_0 was applied at the bottom.

For completeness, the modifications of the triaxial machine, the sample preparation, the saturation procedure,

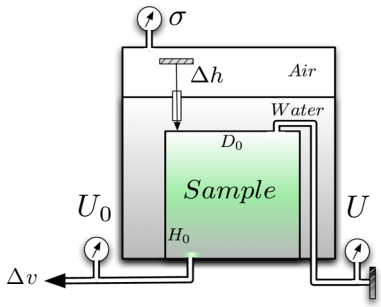

Fig. 2 Sketch of the experimental setup for isotropic compression

the initial void ratio determination by two independent methods, the verification of the anti-frictional system are given in previous works on sands [18,20,21,37]. The effective resolution including actual sensors, electrical cable, data acquisition systems of all transducers are carefully evaluated: ± 0.05 kPa for the pore and cell pressure, $\pm 1.4\,10^{-6}$ for axial strain and $\pm 0.8\,10^{-5}$ for volumetric strain.

Two set of drained isotropic compression tests were designed to study the unconventional instability phenomenon of idealized, fully saturated and very loose granular materials: a first series of 9 tests on very loose samples to inspect the triggering condition of the isotropic liquefaction, randomly ranging from 87 to 316 kPa, the second series of only 4 tests on denser samples to identify the threshold void ratio at the beginning of isotropic consolidation e_{30}^{liq}, leading to a liquefaction-free behaviour during isotropic consolidation up to 500 kPa. A complementary test is performed to compare the newly discovered isotropic instability with the stick-slip instability in drained compression. The average initial void ratio of all samples at fabrication state, e_0, was around 0.750 (solid fraction $\Phi = 0.571$) or a relative density $D_r = (e_{max} - e)/(e_{max} - e_{min})$ of $-57\,\%$ giving an artificially very loose density. The initial bulk density is of about $1.428\ g/cm^3$.

Table 2 summarizes all tests of this study with their initial conditions and their results. e_{30} (respt. Dr_{30}) at the begin-

Table 2 Isotropic consolidation tests on very loose and idealized granular materials

Tests	$e_{30}(Dr_{30})$ (%)	σ'_{trig} (kPa)	Δe	$\Delta\varepsilon_v$ (%)	$\Delta\varepsilon_a$ (%)	ΔU_{peak} (kPa)	ΔU_{stable} (kPa)	f (Hz)	C_c	i	t_{95} (s)
Series A: Liquefaction, global collapse											
I01	0.699 (−11.6)	87	0.0664	3.80	10.7	166	102	88	–	45.50	7.931
I02	0.766 (−71.4)	88	0.0750	4.30	11.3	167	91	83	–	19.17	9.250
I03	0.734 (−42.9)	222	0.0550	3.11	19.3	–	–	–	0.017	–	–
I04	0.702 (−14.2)	282	0.0397	2.22	13.0	414	284	108	0.017	19.60	1.427
I05	0.725 (−35.7)	151	–	–	20.4	261	150	100	–	–	–
I06	0.703 (−15.2)	316	0.0400	2.08	7.63	407	321	27	0.021	15.23	1.032
I07	0.700 (−12.5)	189	0.0360	2.00	7.40	351	195	111	0.016	15.23	0.985
I08	0.713 (−24.1)	267	0.0440	2.44	17.2	307	270	110	0.017	5.73	1.909
I09	0.707 (−18.8)	232	0.0399	2.34	30.3	463	232	70	0.017	25.67	1.116
I10 (*)	0.797 (NA)	496	0.0710	4.10	13.0	990	497	55	0.024	49.60	2.066
Series B: Local collapses											
I11	0.690 (−3.6)	135	0.0130	0.74	0.15	256	122	33	0.018	19.03	0.494
I12	0.677 (8.4)	308	0.0130	0.74	−0.20	275	–	–	0.017	9.78	0.152
I13	0.671 (13.4)	395	0.0148	0.82	−0.28	423	348	91	0.018	8.87	0.168
I14	0.709 (−20.5)	163	0.0102	0.51	0.37	–	–	–	0.021	3.79	–
Drained compression											
CID	0.675 (9.8)	100	0.0362	2.11	13.76	377	299	110	–	–	0.952

(*) on Sili beads

ning of the isotropic consolidation at 30 kPa. σ'_{trig} is the triggering effective isotropic stress of global collapses. Δe the void ratio reduction, $\Delta\varepsilon_v$ the volumetric compaction, $\Delta\varepsilon_a$ the axial contraction, $\Delta U = U - U_0$ the excess pore pressure, ΔU_{peak} the peak of the ΔU in the transient phase, ΔU_{stable} its stabilized value after this transient phase, f the frequency of the transient phase of the pore pressure buildup, C_c the compressibility coefficient, $i = \frac{\Delta\varepsilon_v}{\Delta\varepsilon_a}$ the incremental anisotropic coefficient and t_{95} the time for 5 % of consolidation of this event. Note that test I5 has no volumetric measurement to eliminate the possible influence of the volume sensor compliance and tests I3, I14 cannot capture the ΔU_{peak} due to the storage limitation of the fast acquisition system. For local collapse tests and the drained compression test, σ'_{trig}, Δe, $\Delta\varepsilon_v$, $\Delta\varepsilon_a$, ΔU_{peak}, ΔU_{stable} and f represent the value of the largest collapse.

3 Experimental results

The obtained behaviours for the isotropic consolidation were examined mainly in the traditional compression plane $e-\log\sigma'$, and in the time evolution of σ', volumetric strain ε_v, axial strain ε_a and of excess pore pressure ΔU. According to the soil mechanics convention, volumetric (respt. axial) strains are positive for compaction (respt. compression). For clarity, individual test with numerous collapses is presented separately.

3.1 Spontaneous collapses

The compressibility behaviour of idealized granular materials is shown in Fig. 3 for a typical example in test I04 having $e_{30} = 0.702$, as variation of void ratio e as function of σ' in a semi-logarithmic graph. The short red arrow indicates the time direction. Contrary to the expected smooth and continuous curve of sand media, large unexpected drops in e can be seen, labeled as events A, B and C, occurring successively at 73, 83 and 283 kPa of σ' on the obtained behaviour, thus resulting in a highly discontinuous void ratio variation. The smooth macroscopic compressibility behaviour is interrupted accidentally by a series of successive instabilities. The cell pressure was manually and slowly increased in order to keep the pore pressure generation at a small level, below 4-5 kPa, and to respect the requirement of full drainage for the isotropic consolidation procedure. Since the time between two measurements (hollow circle) is approximately 2 s with the slow data acquisition system for quasi-static behaviour, the compressibility curve indicates a sudden and rapid reduction of σ' at the beginning of each event within 2 s, followed by a more gradual and slowly recover to the previous effective stress level within approximately 6 s; and the effective isotropic consolidation resumes afterwards until the next accident. Note that σ' reduces briefly to a very low level below 3 kPa for all events.

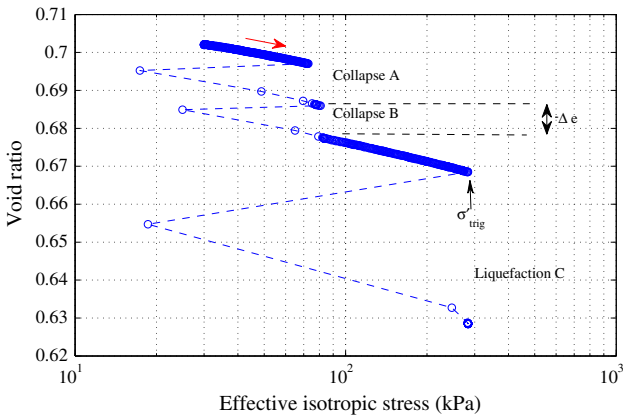

Fig. 3 Spontaneous collapses and liquefaction under isotropic consolidation of test I04 from 30 to 283 kPa with $e_{30} = 0.702$ (color figure online)

While the first two events A and B did not compromise the cylindrical form of the specimen, even with a void ratio drop of 0.0105 for event A, or 0.594 % of $\Delta\varepsilon_v$, the last event C destroyed it with a much larger drop of 0.040 of e, nearly four time larger or 2.110 % of $\Delta\varepsilon_v$, and the granular sample collapsed instantaneously onto the pedestal base of the triaxial cell; hence terminating prematurely the isotropic consolidation test. The third and last event C literally liquefied the sample and offered the first ever recorded spontaneous liquefaction under isotropic consolidation in controlled laboratory in the geotechnical literature, even for idealized granular materials.

For a fully drained isotropic consolidation, this sudden reduction and gradual recover of σ' means equally a sudden and largely unexpected increase of excess pore pressure ΔU, followed by a gradual dissipation due to the drainage system. Fig. 4 shows the evolution of the axial strains, the volumetric strains, the excess pore pressure and the cell pressure as function of elapsed time since the start of the isotropic consolidation test I04. The three events, highlighted in Fig. 3, are shown here with a sudden and simultaneous drop of ε_v and ε_a at the beginning of each event, within the 2 s required by slow and non-synchronized data measuring system. The three narrow and surprisingly very sharp peaks of ΔU are clearly related to these events, despite the usual drainage system with porous bronze disk embedded in the end plates, and indicate a quite fast dissipation. The last peak, well above 250 kPa, was much larger than the two previous ones of about only 60 kPa and presumably responsible for the observed catastrophic liquefaction with a very large run-away $\Delta\varepsilon_a$ of more than 13 % and a sudden volumetric contraction of 2.11 % under less than 2 s. Its significance will be examined later in Sect. 3.3. However, it is not possible to follow precisely the evolution

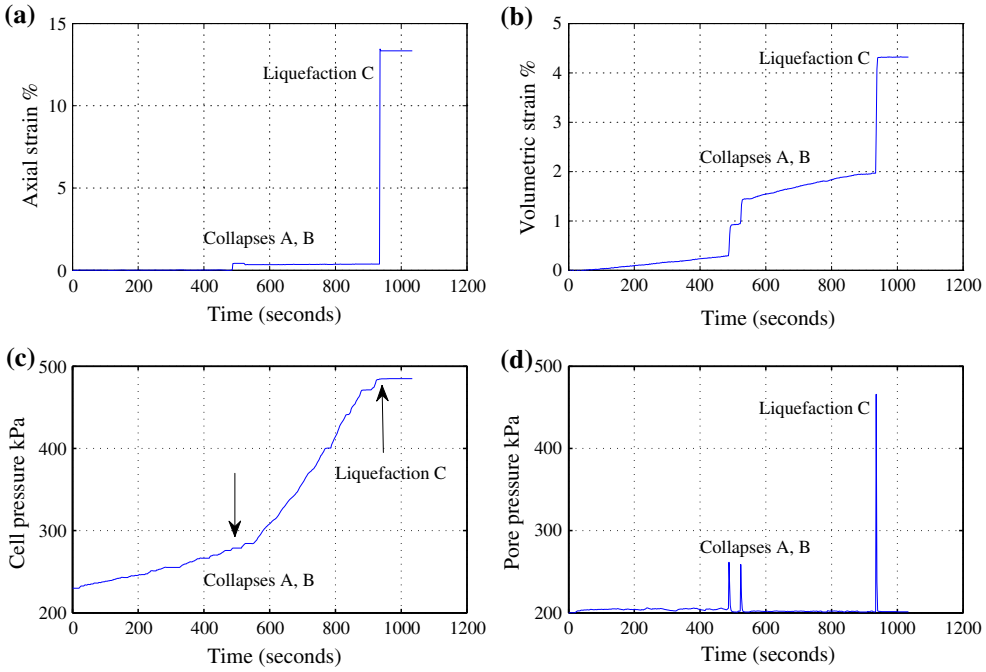

Fig. 4 Axial strain ε_a (**a**), volumetric strain ε_v (**b**), total isotropic stress σ (**c**) and pore pressure U (**d**) as function of elapsed time since the start of the isotropic consolidation test I04. *Vertical arrows* in (**c**) indicate the *onset* of collapses on the evolution of total isotropic stress

Table 3 Collapses and liquefaction under *drained isotropic* compression of test I04

Event	σ'_{trig} (kPa)	ΔU_{slow} (kPa)	ΔU_{fast} (kPa)	Δe	$\Delta\varepsilon_v$ (%)	$\Delta\varepsilon_a$ (%)
A	73	56	119	0.0105	0.594	0.380
B	83	56	126	0.0094	0.466	−0.084
C	283	265	$\geqslant 400$	0.0400	2.110	13.010

in time of these events with the slow data acquisition system. Note the bilinear increasing of the cell pressure with a much faster incremental increase after 280 kPa, due to the manual control. However, the resulting effects on the compressibility behaviour are believed to be negligible due to the fast occurrence of these events practically at constant cell pressure.

The events, defined as characteristic accidents on the triaxial isotropic compressibility behaviour, are associated with sudden and simultaneous drop of ε_v and ε_a, and equally with a simultaneous increase of ΔU or decrease of σ', followed by a gradual dissipation of ΔU or slowly recovery of σ'. These macroscopic parameters are used to characterize irregular events. The first two events are termed as local collapses and the last one global collapse of liquefaction behaviour. A more formal definition of these collapses with viable physical parameters will be assessed in Sect. 4.5. Distinct audible cracking noises were noticed before the appearance of sudden small variation of ε_v on the controlled screen, or even banging noise for final liquefaction event; however, no precise acoustic measurements were attempted in this preliminary study.

Table 3 gives the variations of major parameters $\Delta\varepsilon_v$, $\Delta\varepsilon_a$, Δe and ΔU acquired by the static ΔU_{slow} and dynamic ΔU_{fast} data acquisition system for three main events in a typical isotropic consolidation test.

3.2 Unusual excess pore pressure

It seems that the excess pore pressure ΔU plays a major role in the unexpected spontaneous liquefaction, it was decided to measure its evolution with a faster and synchronized data acquisition system. All key data, i.e. σ'_r, ΔU, ε_v and ε_a were recorded parallel to the existing system and simultaneously with a sampling rate of 2048 Hz to ensure an adequate statistical sampling in the range of 50–200 Hz, the frequency range of presumably engineering interest. The periodic oscillations due to the powerline interference of 50 Hz were filtered out using a simple median filtering and the compressibility behaviour is shown in Fig. 5a, superposing the behaviour measured by the slow acquisition system (red dashed line and hollow circles) with that of fast filtered system (blue line).

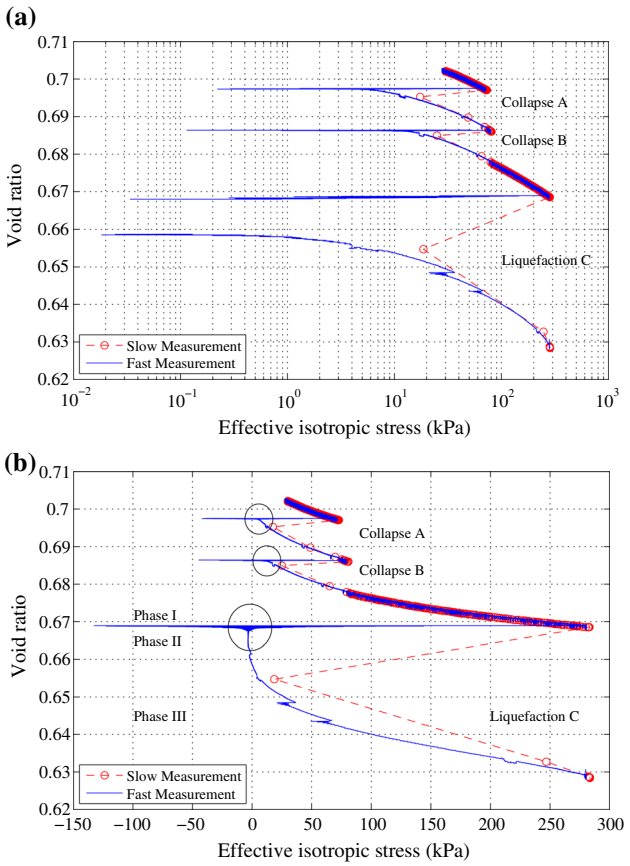

Fig. 5 Spontaneous collapses under isotropic consolidation of test I04, with fast measurements: **a** semilog plot, **b** linear plot (color figure online)

A more complex compressibility behaviour is revealed in this figure, using adequate dynamic acquisition system. The measured data by the two systems, slow and fast, 0.5 and 2048 Hz, are coherent and consistent, offering a more complete picture of the overall behaviour. At the beginning of each event, σ' was first literally reduced and oscillated at constant void ratio, indicated by multiple horizontal lines; then began to recover gradually with a gently curved behaviour, filling all the time gaps of 2 s leaving by the slow acquisition system. The measuring data of the two systems merge at the end of the local collapse and follow the same trend of isotropic compressibility behaviour.

Since the semi-logarithm plot cannot represent the unexpected large positive spikes of measured pore water pressure, resulting in large negative spikes of σ', the complete compressibility behaviour is revealed now using the linear scale for σ'. The dynamic evolution of ΔU of each event can be decomposed in to three phases: a first and fast transient phase I at constant volume and nearly constant axial strain with large spikes ΔU^{peak}, followed by an intermediate second phase II of large increase of volumetric compaction and axial contraction at stabilizing ΔU_{stable} or constant σ' and finally a third and longest phase III of excess pore water pressure dissipation at nearly constant axial strain toward the initial back-pressure of 200 kPa. The time evolution of ΔU of the unexpected transient phase I, especially for liquefaction event C (black hollow circles), will be examined later in Sect. 3.3. The first two events, representative of local collapses, do not have the second phase II of constant σ', while the lengthy and slightly negative value of σ' constant due to median filtering of volumetric data of the last event is responsible for the global liquefaction phenomenon. Their local collapses are relatively insignificant compared to the last catastrophic one. Small events or aftershocks can even occur in the dissipation regime, as indicated by two minor events happening around 30 and 60 kPa.

Despite the fully drained system, phase I occurs in undrained conditions, phase II in drained and phase III in mixed conditions of consolidation.

3.3 Instabilities as dynamical events

The individual time evolution of ΔU of the first two events A and B is captured separately in Fig. 6, with emphasis on the fast transient phase I with sudden outburst lasting <0.2 s. They share the same characteristics of dynamic vibration with very fast and sudden rising time to U_{max} of the first peak within only 5 ms, the relatively fast decay to stabilizing ΔU_{stable} within 200 ms, and the lengthy dissipation in the range of 5 to 8 s (not shown in figure). This figure can explain why the slow pace of 0.5 Hz of measurement system fully missed the very short-lived peaks and the stabilized value of ΔU. Furthermore, since the pore pressure transducer is on the other side of the porous bronze disk of the top cap, connected with rigid and thick plastic tube, the actual value of these sharp peaks, revealed by fast measurement system, is likely a minimum estimate.

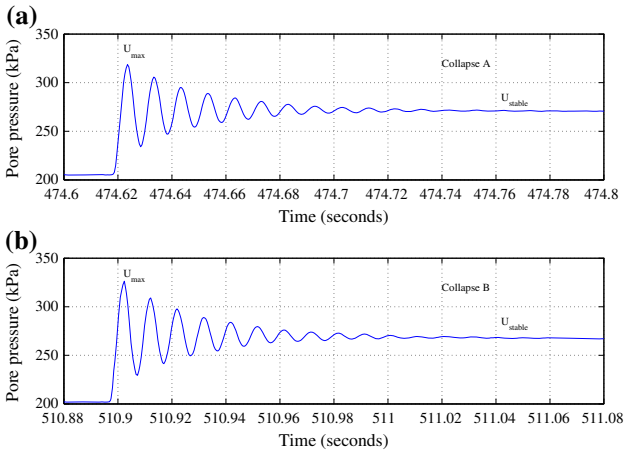

Fig. 6 Time evolution of fast transient phase I of pore water pressure of event A occurring at 73 kPa (**a**) and B at 81 kPa (**b**) of test I04

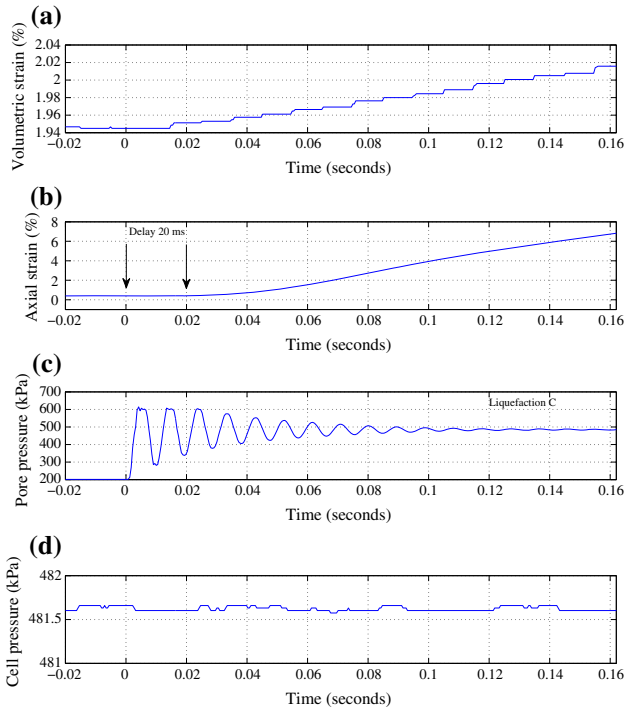

Fig. 7 Time delay between volumetric strain (**a**), axial strain (**b**) pore water pressure (**c**) and cell pressure (**d**) of liquefaction event C occurring at 283 kPa of test I04

For the liquefaction event C, Fig. 7 shows clearly the time delay of about 20 ms between the sudden rise of ΔU and the beginning of the gradual progression of axial strain and of volumetric strain. The time origins are coincided with the beginning of the sudden development of ΔU. The stabilization of the cell pressure shown in Fig. 7c is within a small variation of only 0.2 kPa. Figure 7 strongly suggests the excess pore pressure as the initial cause of the development of ε_v (top) and ε_a (middle). Unfortunately, electrical noises prevent the proper identification of this time delay for smaller events A and B.

As an example, the dominant frequency in the range of 80-140 Hz with a loosely defined peak of about 102 Hz of the liquefaction event is identified in Fig. 8, using Fast Fourier Transformation on a time window of 700 ms of data centered on the first rising of ΔU.

To check that the transient vibration is not an artefact of the measurement system, a dynamic pore pressure sensor (PCB S112A21) having high resonant frequency (250 kHz) was used together with the static one on the same location, separated by a short distance of 10 cm. No difference was detected.

The excess pore pressure was normalized by the stabilizing ΔU_{stable} to eliminate the dependency on ΔU_{stable} and Fig. 9 shows the normalized results of ΔU^{norm}, with the origin shifted to the beginning of the transient phase ±0.5 ms, which is the current time resolution. This normalization enables the study of different events, independently of ΔU_{stable} and σ'_{trig}, as in Fig. 10. The events seem to share the same dynamic characteristics of an underdamped free

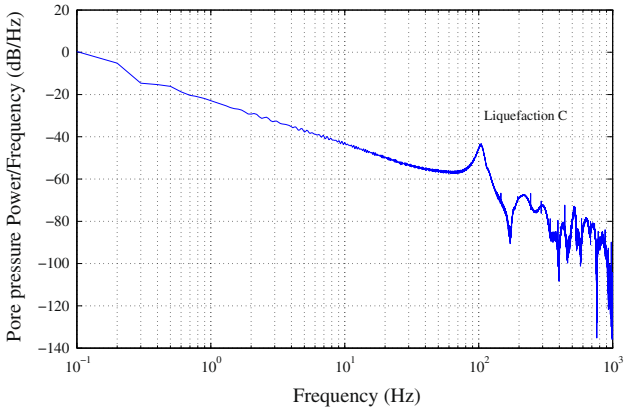

Fig. 8 Vibration frequency in the range of 80–140 Hz of pore water pressure at liquefaction event of test I04

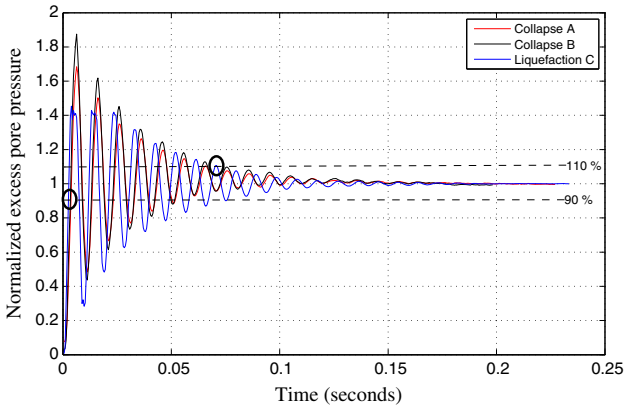

Fig. 9 Normalized transient behaviour of pore water pressure for all events of test I04

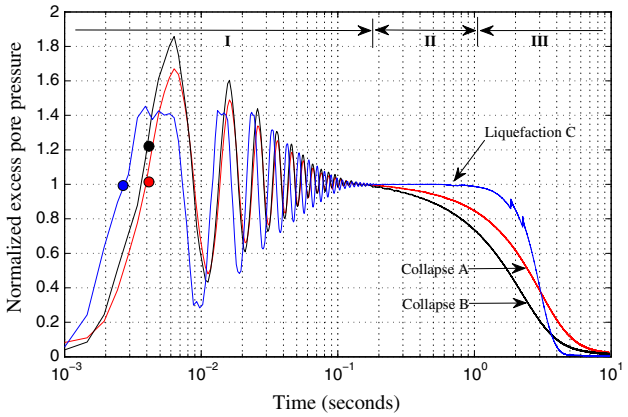

Fig. 10 Three phases of pore water pressure development: I fast buildup, II constant stable (liquefaction) value and III dissipation (post-liquefaction). Inferred liquefaction points (*solid circles*) are indicated

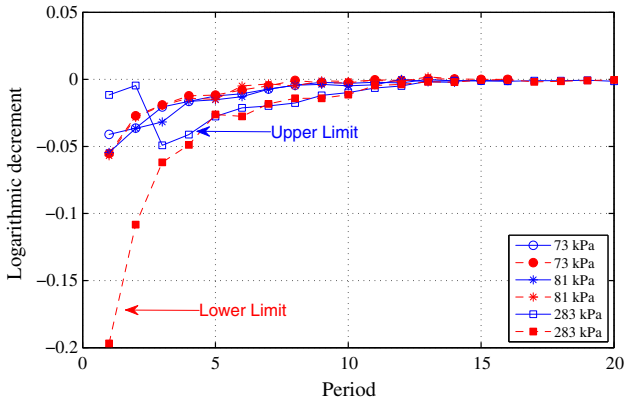

Fig. 11 Decaying characteristics of transient behaviour of pore water pressure of test I04

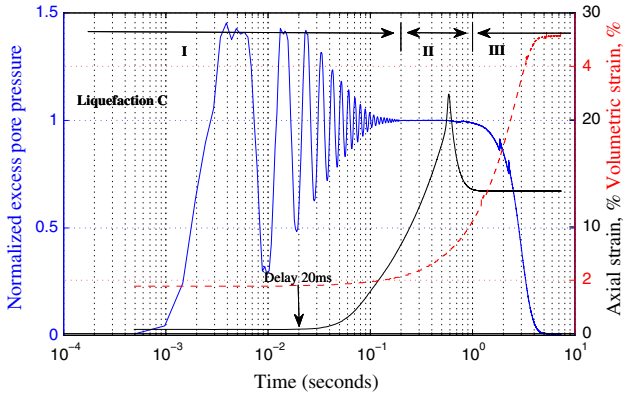

Fig. 12 Normalized behaviour of pore water pressure, axial strain and volumetric strain for liquefaction event of test I04

oscillating system, regardless of ΔU_{stable}: approximately a same range 80-140 Hz of vibration frequency, a same very fast rise time of less than 3 ms to reach 90 % of the normalized steady-state value $\Delta U^{norm}_{stable} = 1$, and a same dissipated time of about 150 ms to attain ΔU_{stable}. However, different settling times in the range of 70–90 ms to remain within $\pm$ 10 % of the steady value ΔU_{stable} (hollow circles for event C) were identified. Note that the total number of oscillations increases slightly with increasing σ'_{trig}, from 12 to 18.

Grouping together the ΔU^{norm} of all events, Fig. 10 gives the time evolution of pore pressure and delineates a clear temporal separation of 3 phases: a fast transient phase *I* lasting only 150 ms, a stable isochoric phase *II* presented only in liquefaction event and a long dissipated phase *III* or post-liquefaction. For catastrophic event C, phase *II* denotes the liquefaction and phase *III* the post-liquefaction, characterized by the greatest slope of the dissipation curve. The superimposed liquefaction points (solid circles) indicate the ΔU^{norm} levels inferring a null effective stress. For liquefaction event C, the ΔU^{norm} level is exactly equal unity, meaning a null effective stress for the whole phase *II*, hence the liquefaction phase.

It seems that ΔU is not homogeneous during the transient phase. Consequently, the magnitude of σ' may be misestimated since it depends on the measurement position of the pore pressure sensor. However, full liquefaction is undoubtedly detected.

Figure 11 gives the logarithmic decrement representing the decay of the ratio of two successive normalized excess pore pressure peaks, above and below ΔU_{stable}, labelled as upper limit and lower limit. All events have a gradual reduction to zero of this logarithmic decrement. Nevertheless, each event has its unique decaying rate, depending on σ'_{trig}, independently of the upper and lower peaks.

Additional information can be found when examining together the time evolution of ΔU, ε_v and ε_a in Fig. 12 with semi-logarithmic scale for the catastrophic event C.

The axial strain shows a very strange behaviour. Indeed, while the slow temporal evolution of ε_a in Fig. 4a indicates a sudden jump to 13 %, a more accurate measurement reveals a fast axial contraction, after a small delay of 20 ms with respect to ΔU, up to 22.30 % from 0.43 % within only 0.6 s, followed by an axial extension towards a stable value of 13.28 %, or an vertical extension of 9.02 % in 0.5 s. This vertical compression indicates an axial strain rate $\dot{\varepsilon_a}$ of about 36.45 %/s (1531 mm/min), much faster (7655 times as fast as the usual constant $\dot{\varepsilon_a}$ of 0.0048 % (0.2 mm/min) in triaxial compression experiment). It clearly indicates a dynamic regime of the liquefaction phenomenon happening within less than 1 s. This axial rebound is very unexpected for an isotropic consolidation. Unfortunately, no suitable explanation can be found for this particular aspect. Note also that a large axial contraction of about 8 % is already occurring during the transient phase *I* of 200 ms.

The volumetric strain indicates an overall contraction of only 2.34 % during liquefaction, with a similar initial time delay and its development is far behind that of axial strain, both in terms of time evolution and of magnitude. The liquefaction event, encompassing phases *I* and *II*, suggests the first fast granular phase transition from solid to liquid with increasing grain separation towards the ultimate situation of no contact between grains. The null state of effective stress combined with the vertical direction of natural grain weight can explain the very large axial contraction (20 %) comparing to the radial expansion (−9 %). The post-liquefaction event of phase *III* suggests the second relatively slow reversing granular liquid-solid phase transition with regaining grain contacts due to the hollow cylindrical elastic membrane.

These important observations highlight the dynamic character of all three events, in Table 4, correlated to the sudden surge of excess pore pressure and related likely to the slip

Table 4 Dynamic characteristics of pore pressure development

Event	σ'_{trig} (kPa)	ΔU_{max} (kPa)	ΔU_{stable} (kPa)	Osc.	f (Hz)	Stabilization (ms)	Dissipation (s)	Offset (ms)	e_{trig}	Slope
A	73	119	72	12	102	200	8	0	0.697	1.285
B	83	126	68	13	102	200	6	0	0.686	1.285
C	283	$\geqslant$400	285	18	102	200	5	18	0.669	3.587

instability of the stick-slip phenomenon during shear [19]. Unfortunately, as in the case of stick-slip instabilities, they give no clear indication about the physical triggering mechanisms of ΔU.

3.4 Compressibility parameters

Upon ignoring the local collapses, a unique and continuous compressibility behaviour is retrieved in Fig. 13 by artificially shifting upwards at σ'_{trig} by Δe from Fig. 3, closing the void ratio gap created by spontaneous collapses and linking together two largest linear segments in Fig. 3 which reveals a hypothetical mechanical behaviour conforming to the usual isotropic or one-dimensional compressibility of loose sand materials without unloading under fully drained conditions [80]. As usual in soil mechanics, the compressibility behaviour can be approximated by two straight lines representing the normal compression line and the unloading-reloading line. The initial portion of the curve is usually flatter and has the same slope of the unloading line. The intersection point of these two lines defines the preconsolidation stress σ'_p as a reminder of the past maximum vertical effective stress.

Some macroscopic compressibility parameters can be identified: a compression index $C_c = \Delta e/\Delta log\sigma' = 0.017$ for loading, a swelling index $C_s = \Delta e/\Delta log\sigma' = 0.014$ for unloading and an apparent preconsolidation stress $\sigma'_p = 60$ kPa created logically by the under-compaction method. The usual preconsolidation stress in saturated condition would be lower, since the initial compaction was done in unsaturated state. Note that loosely bound glass beads have a particular isotropic compression behaviour with $C_s \approx C_c$, in contrast with real granular materials where $C_s \approx C_c/10$. This observation confirms the quasi-reversibility behaviour for model granular materials numerically obtained in [2,59,69] using discrete element modelling (DEM), however, without the unexpected collapses and liquefaction. Glass beads assess a more non linear elastic behaviour than sand materials. This straight line of slope C_c representing the compressibility behaviour of the classical drained isotropic compression of geomaterials is no longer respected; it was interrupted accidentally by a collection of events with fast transition from undrained to drained loadings in Figs. 3, and 5.

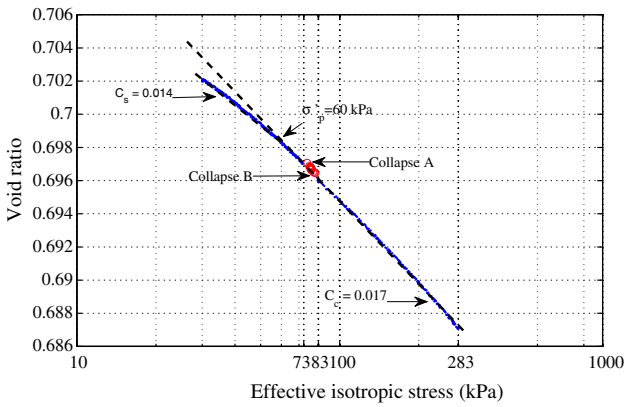

Fig. 13 Classical compressibility parameters under isotropic consolidation of test I04 upon ignoring local collapses

The individual compression index C_{ci} can be estimated for three continuous segments in the actual compressibility behaviour of Fig. 3, resulting in a very similar value of about = 0.017, independently of the void ratio occurring at the beginning of the segment. Constant C_{ci} means the compliance of glass beads, besides the collapses, with the classical critical state of soil mechanics [67].

The hypothetical behaviour of Fig. 13 indicates a combined and continuous void ratio reduction $\Delta e_{iso} = 0.0148$ due to the quasi-static isotropic consolidation alone, totaling only 24.7 % of the total reduction of the three unusual collapses $\Delta e_{collapse} = 0.0599$. Even combined, it is still smaller than that created by final collapse, totaling only 37.0 %. As expected, the biggest void ratio reduction came from the liquefaction phenomenon, as well as the biggest volumetric compaction and the biggest axial contraction. Without the collapses, the void ratio at the end of the isotropic consolidation at 287 kPa would be in a very loose state of $e_c = 0.692 (Dr_c = -5.4\%)$, instead of a medium dense state of $e_c = 0.632 (Dr_c = 48.2\%)$.

A practical consequence is the impossibility to control the void ratio reduction under isotropic consolidation of very loose and moist-tamped idealized granular materials, due to the random occurrence of the dynamic instabilities, unless mastering the triggering mechanisms.

It is worth noting that this isotropic consolidation gives a rather large incremental anisotropic coefficient $i = \frac{\Delta\varepsilon_v}{\Delta\varepsilon_a} =$ 19.6, contrasting sharply the isotropic structure $i \approx 3.0$ for loose laboratory sands (i.e. Hostun or Toyoura) created by the same moist-tamping procedure [24]. This initial, strongly

structural anisotropic state of an assembly of spherical particles can be the results from preferred orientation of unit vectors normal to contact surfaces [64].

3.5 Undetermined liquefaction and instabilities

The unusual experimental findings in the previous section are nicely applied to all tests of the first series. The isotropic compressibility shown in Figs. 14 and 15 for different tests of series A having nearly the same $e_{30} = 0.718 \pm 0.023 (Dr_c = -28.4 \pm 20.8\,\%)$ of this study highlights the random nature of the triggering stress leading to liquefaction, ranging from 87 to 324 kPa; as well as the number and the triggering stress of intermediate local collapses. For clarity, each test is shown separately.

The occurrence of isotropic triggering stress σ'_{trig} is distributed over a wide range. It can be as small as 87 kPa, in two cases shown in Fig. 14 without any preceding local collapses, or as large as 316 kPa in Fig. 15c with numerous preceding local collapses or precursors. Notice that no more than 4 local

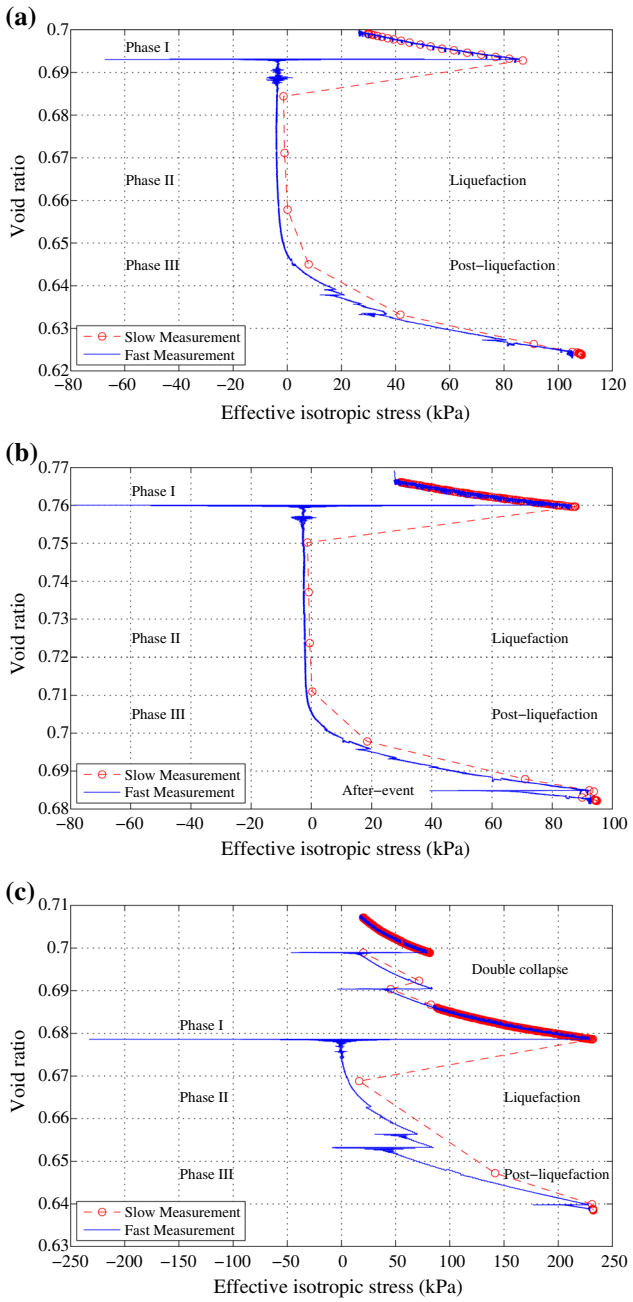

Fig. 14 Isotropic liquefaction **a** at 87 kPa and $e_{30} = 0.699$ of test I1, **b** at 88 kPa and $e_{30} = 0.766$ of test I2, **c** at 232 kPa of test I09

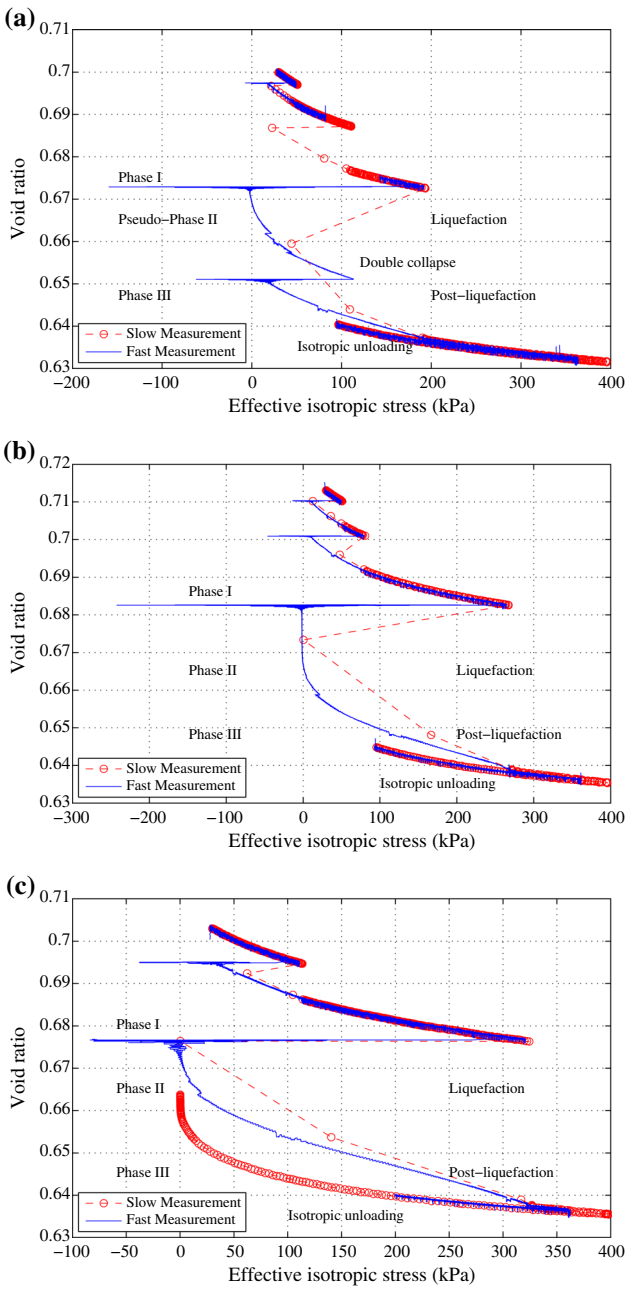

Fig. 15 Isotropic liquefaction **a** at 189 kPa of test I07, **b** at 267 kPa of test I08, **c** at 316 kPa of test I06

collapses were observed before the final liquefaction for all tested samples. Another practical consequence is the possibility of ending the isotropic consolidation before attaining 100 kPa, or even 300 kPa and to subsequently perform the usual series of shearing test in compression, either in drained or in undrained condition, as in [19]; however, with no clear confidence of a well behaved isotropic testing.

Three experimental observations can be made from Fig. 14. The most obvious is the unusual large void ratio reduction under constant σ' of the second phase for more than 8 s, for tests I01 and I02, therefore detected by the slow acquisition system. The second observation concerns the multiple aftershocks at the beginning of phase *II*; it can be interpreted as immediate, however minor, multiple rearrangements of granular structure. The third one points to the existence of a large aftershock in the post-liquefaction regime, at the end of the pore pressure dissipation of test I2. However, the amplitude of pore pressure of the aftershock is not enough to re-liquefy the sample.

These figures confirm the broader positive spikes of measured ΔU for all events, creating largely negative spikes of σ' and triggering the liquefaction, the decomposition of three phases of ΔU with emphasis on the lengthy second phase, responsible for liquefaction, along with its absence for intermediate collapses and additional secondary collapses. It would be tempting to relate the apparently repeatability of having two isotropic liquefaction occurring at the nearly same stress state of about 87 kPa to pure coincidence. Perhaps the most logical response concerns the same internal granular microstructures, likely created by the same fabrication technique, developed later in Sect. 4.5.

Figure 15a shows the first and the only observed occurrence of double successive local collapses in this series, leading to the liquefaction at 189 kPa even in the absence of the second phase of constant σ'. The second collapse occurs at 112 kPa, below the initial σ'_{trig}, well before the end of the consolidation phase and is not detected by the slow acquisition system. Without this second collapse, it would be able to end correctly the isotropic consolidation beyond 300 kPa. Since the sample is still in an upright position, even after experiencing double collapses with large axial strains of about only 7.4 %, it can sustain the isotropic loading up to 400 kPa and unloading down to 100 kPa to create the overconsolidation state with OCR = 4. Additionally, this test shows the not so granted possibility of having isotropically overconsolidated sample of loose glass beads. The particular quasi-elastic behaviour of loosely bound glass beads with $C_s \approx C_c$ is clearly illustrated in this figure.

Figure 15b, c confirm the above observations with spontaneous liquefaction at high isotropic stress of 264 and 324 kPa, accompanied with only two and one precursors.

It is worth noting that there is virtually no visual sign of strain localization and the sample shape remains almost

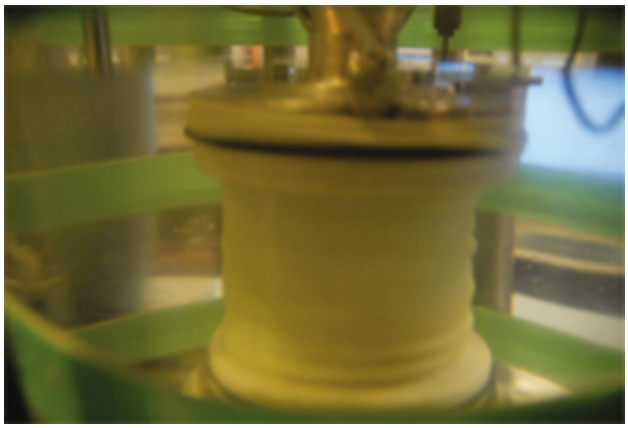

Fig. 16 Upright position after full liquefaction state with sudden jump 14 % of axial strain

cylindrical, as expected for isotropic loading. Since the reported mechanical measurements are not coupled with a visualization technique, no direct confirmation is possible within this paper. However, Alshibli and Roussel [3] also noticed the absence of localization on medium dense assemblies of model granular materials in triaxial compression using X-ray tomography. Figure 16 shows a rare case in our tests where a sample still stands in an upright position, after experiencing a large and sudden axial jump of about 14 % during spontaneous liquefaction. The presence of numerous horizontal water pockets in the lower part of the latex membrane assesses the vanishing effective stress state. The dynamic instability of glass bead assembly might be associated with the diffuse failure for undrained [14] and drained [66] behaviour for loose sand.

The time evolution of individual ΔU of each test event in the liquefaction series A is shown separately in Fig. 17, for clarity, together with the inferred liquefaction levels. These results confirm the usefulness of the normalized procedure to eliminate the effects of ΔU_{stable}, the spontaneity of the pore pressure development without any visible external source, the separation of three distinct phases, the always present transient oscillatory phase *I*, the lack of phase *II* for local collapses and the very short time duration of about 1 s for the liquefaction phenomenon. The greater slopes of all post-liquefaction events indicate a fast dissipation regime, comparing to the slower ones of local collapses.

Note that spontaneous liquefaction also randomly occurs at the end of saturation stage for some tests under 20 kPa of isotropic pressure.

The spontaneous instabilities could occur more frequently, and probably accompanied with large magnitude of U^{peak}, facilitated by the use of pore fluids having higher viscosity [9]. The possibility and the occurrence of liquefaction could be different. However, this particular aspect remains beyond the scope of this paper.

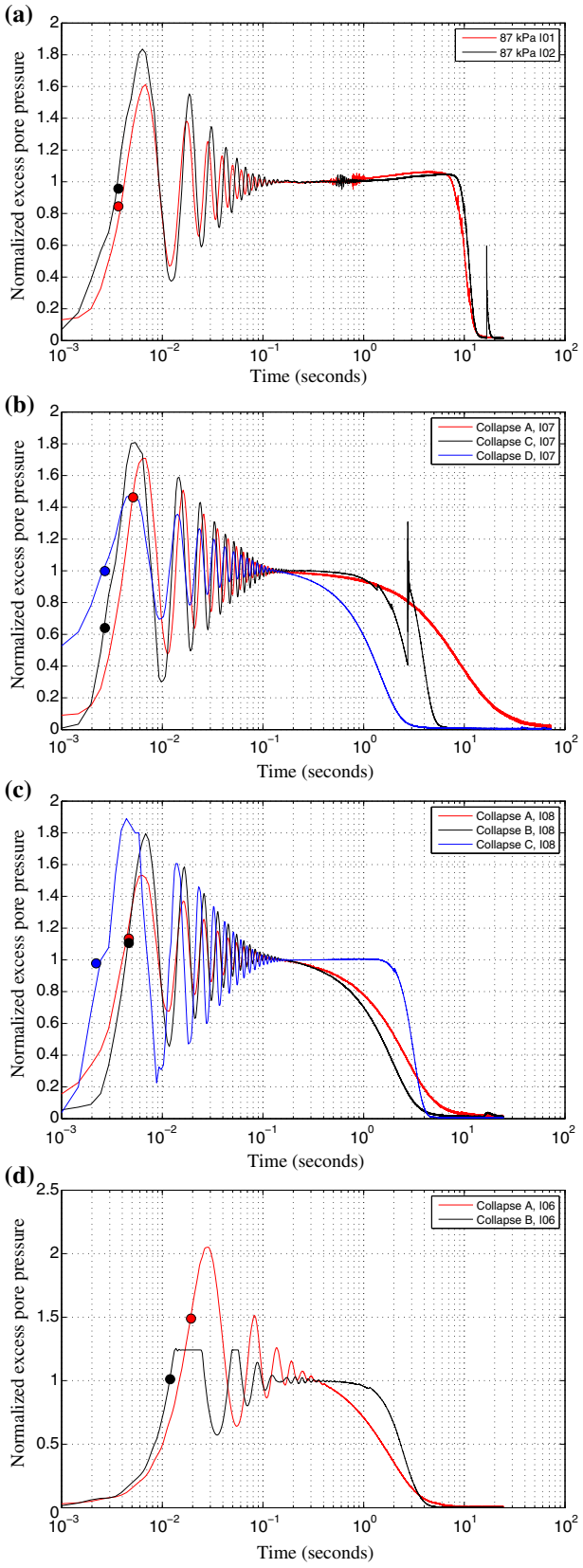

Fig. 17 Pore pressure evolution of collapse events of **a** tests I1 and I2, **b** test I07, **c** test I08, **d** test I06

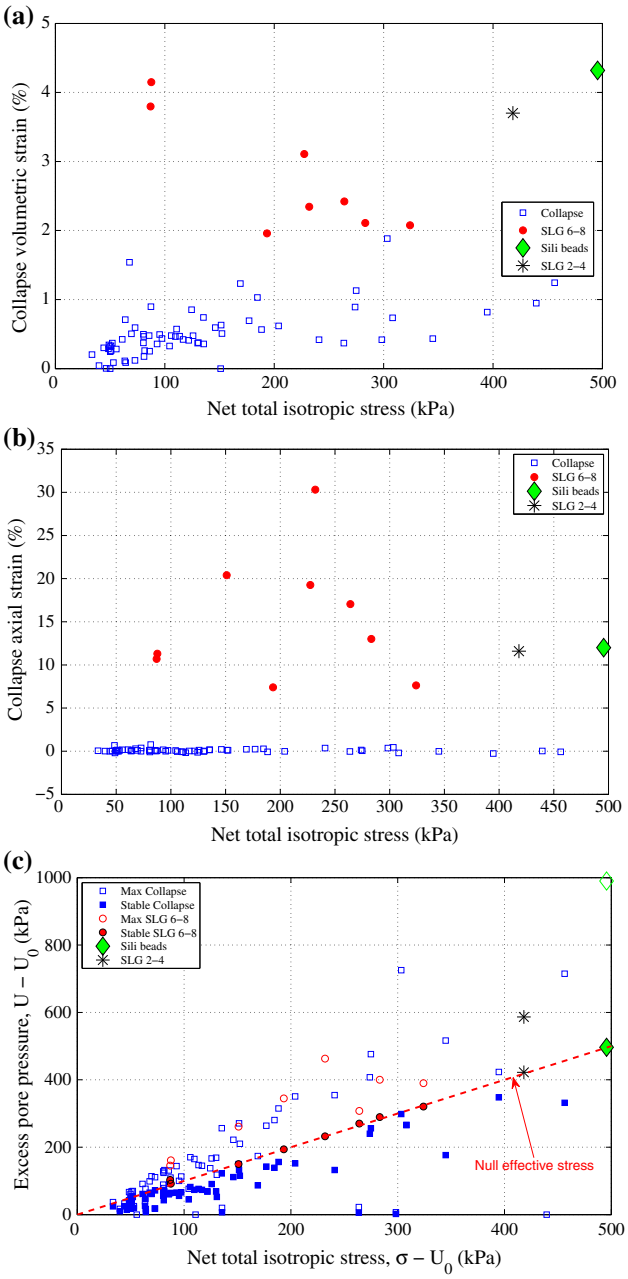

Fig. 18 Effects of σ'_{trig} on isotropic collapses and liquefaction **a** volumetric strain, **b** axial strain, **c** excess pore pressure (color figure online)

3.6 Effects of changes in σ'_{trig}

Table 2 gathers together the macroscopic parameters in all occurrences of isotropic liquefaction; and Fig. 18 displays the dependency of σ'_{trig} on the measured macroscopic parameters of each event, $\Delta\varepsilon_v$, $\Delta\varepsilon_a$, ΔU^{peak} and ΔU_{stable}. The numerous small local collapses in hollow blue squares outnumber the few and large global liquefaction in full red circles and constitute clearly a separate group for $\Delta\varepsilon_v$ in Fig. 18a and $\Delta\varepsilon_a$ in Fig. 18b. However, the data shows no clear tendency,

excepting for an approximately linear increasing trend of $\Delta\varepsilon_v$ for local collapses with increasing σ'_{trig}, with relatively low correlated factor of only 0.53, and for small amplitude of $\Delta\varepsilon_a$, between ± 1 %. Large confining pressure tends to create large volumetric compaction for local collapses; and it seems that unexpected small axial extension was randomly recorded in the lower half portion of Fig. 18b, scattering all over the whole range of effective confining pressure. This particular axial extension can be probably related to the inclination of the top plate, therefore to the inhomogeneous state of specimen.

The measured transient ΔU^{peak} (hollow symbols) is largely and briefly located above the diagonal red line representing the state of null effective stress where the excess pore pressure ΔU equals the total confining pressure σ_3 in Fig. 18c. It can be speculated that the brief duration of ΔU^{peak} in the range of 150 ms is enough to initiate the liquefaction phenomenon and not enough to maintain its development and then to propagate the local liquefaction onto the whole sample. The stabilized values ΔU_{stable} (full symbols) for all local collapses are below or near this line; and those of large events are precisely on this line for a more lengthy time of about 6–8 s, creating the stress state of null σ' during the second phase of pore pressure development and therefore triggering and sustaining the catastrophic liquefaction phenomenon.

4 Analysis of spontaneous liquefaction behaviour

In the rest of this paper we now focus on a global view of this very unconventional phenomenon of spontaneous liquefaction under isotropic consolidation, trying to answer some specific questions: Can we have a liquefaction-free behaviour? What are the necessary conditions leading to the unexpected isotropic liquefaction? Can we identify the possible driving physical mechanisms behind these dynamic instabilities? And more importantly, what are the triggering mechanisms of the liquefaction phenomenon?

4.1 Threshold fabric void ratio

Since the first test series concerns only very loose materials to better stimulate the appearance of liquefaction, the next logical step is to investigate the dependency of the isotropic liquefaction potential on the void ratio by increasing gradually e_o at fabrication state, hence indirectly e_{30} at the beginning of the isotropic consolidation at 30 kPa. The compressibility behaviour shown in Fig. 19a–c indicates the total disappearance of liquefaction of denser samples below $e_{30} = 0.690$.

From these figures, at least three additional observations can be made. First, although the absence of total failure by

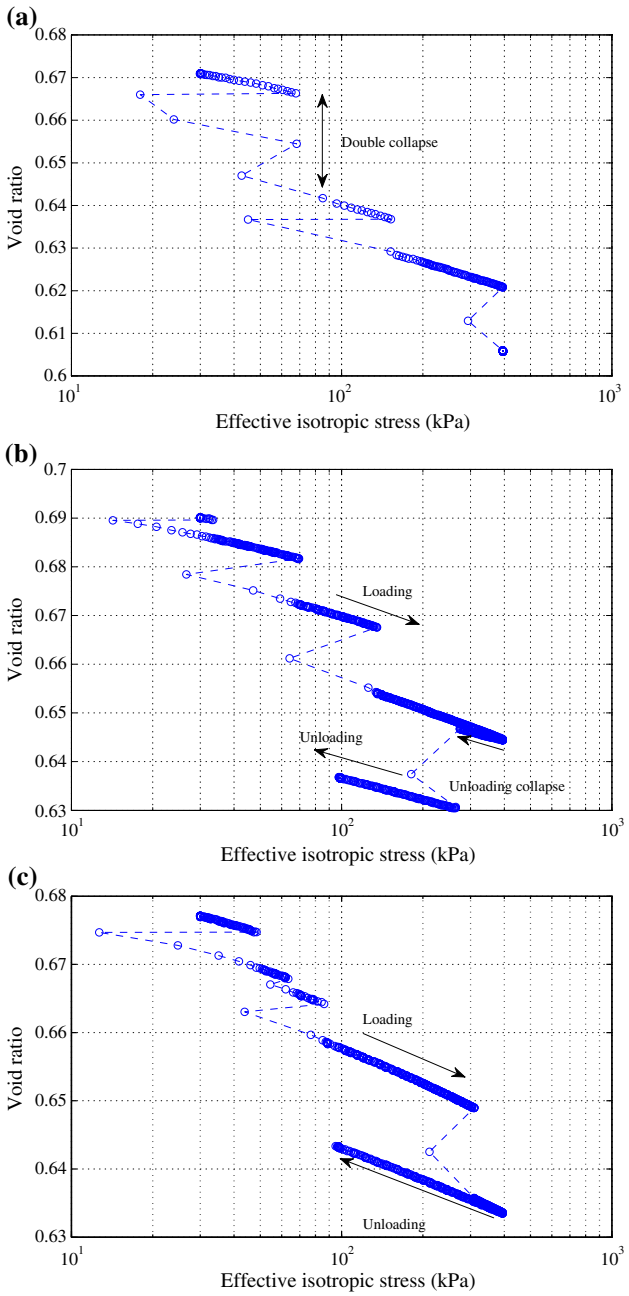

Fig. 19 Isotropic consolidation without liquefaction for dense sample below e_{30}^{liq} **a** $e_{30} = 0.671$ of test I13, **b** $e_{30} = 0.690$ of test I11, **c** $e_{30} = 0.677$ of test I12

liquefaction is of particularly note, the σ' is briefly vanished in the transient phase *I* and even a small value below 2 kPa is recorded by the slow acquisition system. The brief reduction of σ' is not enough to sustain a liquefaction state. Faster system confirms the absence of phase *II* on the pore pressure development. The second observation taken from Fig. 19a is the sample's survival after a double local collapse resulting in a rather large axial contraction and volumetric compaction. The third and major observation concerns the occurrence of large local collapse in unloading in Fig. 19b. This is the first

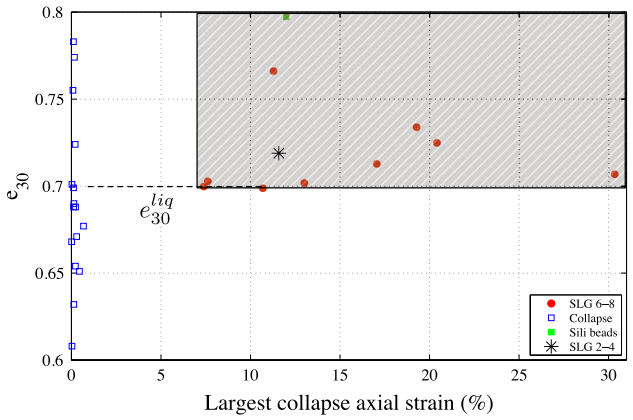

Fig. 20 Identification of threshold void ratio e_{30}^{liq} indicating a total disappearance of liquefaction on denser samples (color figure online)

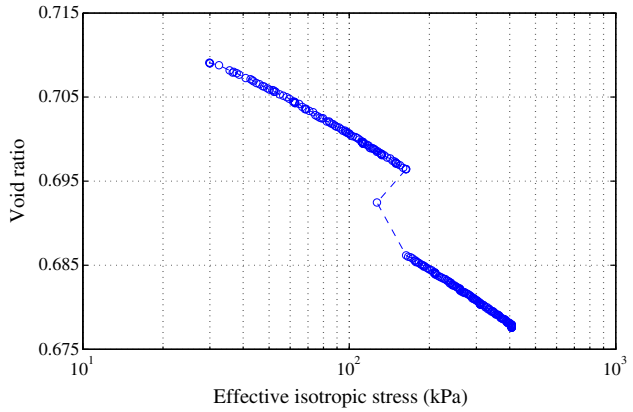

Fig. 21 Isotropic consolidation from 30 to 400 kPa without liquefaction for loose sample above e_{30}^{liq} with $e_{30} = 0.709$ of test I14

and the only reported unstable behaviour during isotropic unloading in the entire experimental program.

Combined with the results of first test series, this trend exhibits the liquefaction phenomenon above a liquefied fabric void ratio e_{30}^{liq}, representing the transition from global instability with total breakdown to local instability with partial collapse and liquefaction-free during isotropic consolidation in Fig. 20. This threshold void ratio can be narrowed down to $0.690 \leqslant e_{30}^{liq} \leqslant 0.699$ ($-3.6 \geqslant Dr_{30}^{liq} \geqslant -11.6$) using the data in Table 2. Since it is inherently difficult in practice to control e_{30} due to the undetermined nature of the instability phenomenon, no attempt was made to locate precisely e_{30}^{liq} with additional tests.

However, it should be noted that the found e_{30}^{liq} is not a full proof guaranteeing the total absence of isotropic liquefaction. Loose glass bead assemblies with $e_{30} \geqslant e_{30}^{liq}$ can be exempted of total liquefaction. A liquefaction-prone sample in Fig. 21 with $e_{30} = 0.709$, slightly above e_{30}^{liq}, shows only one local collapse occurring at 163 kPa. It just strongly suggests the possibility of avoiding the total failure below e_{30}^{liq} since none of 15 tests (not shown in this paper) below this limit exhibits liquefaction. Having an initial void ratio denser than e_{30}^{liq} is currently a practical way to better prepare for a liquefaction-prone isotropic consolidation.

Monodisperse glass beads, initially assembled in a very loose state by moist-tamping technique, experience only local collapses during the complete isotropic consolidation from 20 to 500 kPa. Even no collapses at all can be found for denser samples below e_{30}^{liq}.

The threshold void ratio e_{30}^{liq} can be related to another threshold void ratio $e_c \approx 0.934$–0.936 ($7.0 \geqslant Dr_c \geqslant 6.4$), guaranteeing a liquefaction free behaviour during subsequent undrained shearing for very loose Toyoura sand [17,75]. In the geotechnical literature, e_c represents the transition from liquefaction behaviour in undrained shearing to non-liquefaction behaviour characterized by the classical steady state of deformation (SSD) [12].

4.2 Global compressibility characteristics

Interestingly and logically, upon ignoring the local collapses, the two test series indicate a unique and global isotropic compressibility behaviour, independently of e_{30} in the range of 0.766 to 0.671 (or Dr_{30} varying from -71.4–$13.4\,\%$). The mean values for the compressibility macroparameters are: $\langle C_c \rangle = 0.018$, $\langle C_s \rangle = 0.012$, $\langle \sigma'_p \rangle = 60$ kPa. Note that $\langle C_s \rangle \approx \langle C_c \rangle$, reconfirming the quasi-reversible behaviour for model granular materials.

4.3 Spontaneous liquefaction characteristics

Figure 22a shows the transient behaviour of normalized ΔU for all liquefied events, including the special drained shear test in triaxial compression of Sect. 4.7, with the presence of one large aftershock in two events. As noticed before for test I04 in Fig. 9, the same dynamic characteristics of a underdamped free oscillating system were retrieved for series A: a mean vibration frequency of 100 ± 12 Hz, a maximum value of ΔU_{max}^{norm} of about 1.8, a rise time of 2.4 ± 0.8 ms and settling time 64.6 ± 8.8 ms excepting for test I06. These nearly identical characteristics probably denote a same underlying phenomenon, triggered by the same physical mechanisms for a test series with nearly constant e_{30}.

Upon ignoring the transient oscillatory phase I, for ease of thinking, a mean pore pressure development $\langle \Delta U^{norm} \rangle$ can be constructed (thick blue dashed curve), merging the two phases I and II. The liquefaction is initiated as early as 3 ms from the beginning of pore pressure rise and the null effective stress state maintained for at least 1 s before the final dissipation stage. Currently, additional experiments will be needed to verify if the observed transient phase is due to the experimental setup or to the material characteristics.

The corresponding axial and volumetric strain are shown in Fig. 22b, c, with the origin shifted to the steady-state

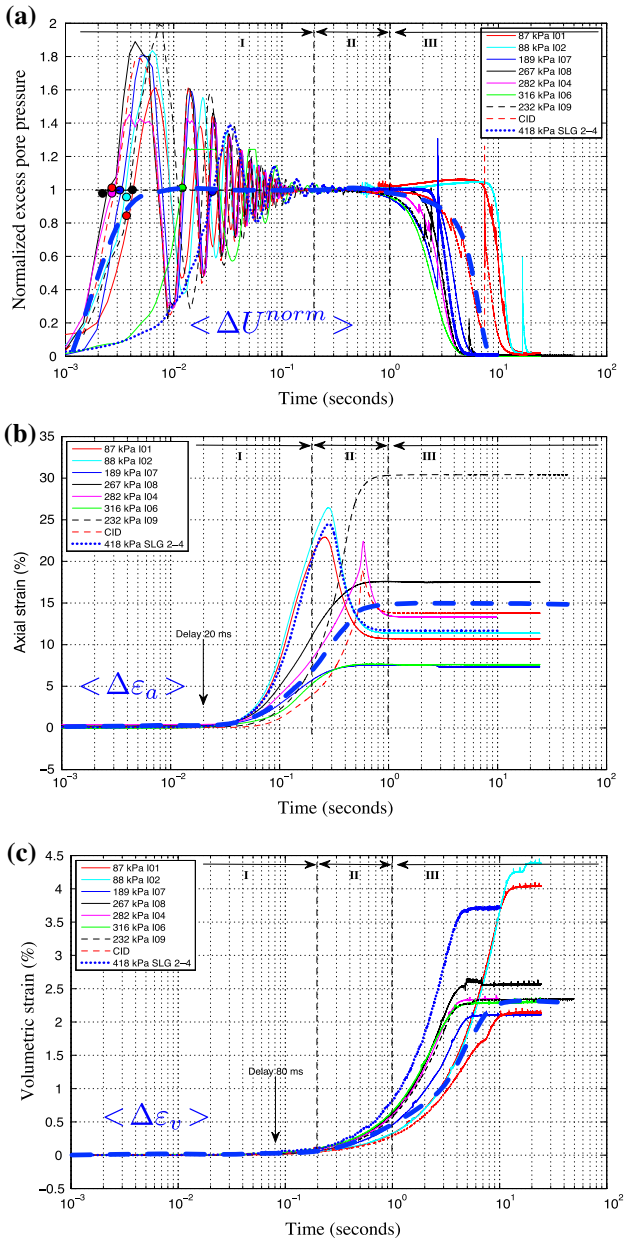

Fig. 22 Isotropic liquefaction **a** normalized transient behaviour of excess pore water pressure, **b** axial strain, **c** volumetric strain (color figure online)

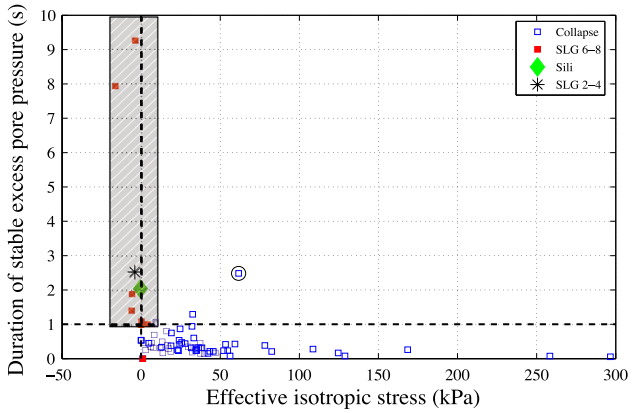

Fig. 23 Conditions for liquefaction event

value before liquefaction event, for clarity. These figures emphasize the lack of simultaneity between ΔU or σ' and $\varepsilon_a, \varepsilon_v$. A quite large variation of final steady-state value is observed for both ε_a and ε_v and the unexpected axial rebound is noticed for half of the series. The axial strain rate $\dot{\varepsilon_a}$ varies vastly from 19.60 %/s (13.7 mm/s) to a tremendous rate of 130.50 %/s (91.4 mm/s) of tests I01 and I02 while the volumetric strain rate $\dot{\varepsilon_v}$ changes only mildly from 0.284 %/s (0.76 cm^3/s) to 0.692 %/s (1.86 cm^3/s). Even with the axial rebound, a mean temporal behaviour can be drawn. At any strain rate, the axial collapse occurs first entirely in the range of only 0.1–0.5 s, from the sudden beginning of pore pressure development, while ε_v lags slowly behind in the range of 3–8 s, clearly in the dissipated phase *III* or post-liquefaction. The consequence is once the pore pressure triggered and sustained the stable state ΔU^{norm}_{stable} for at least 0.5 s, it is impossible to stop the catastrophic global axial collapse within this very short time duration. The current leading hypothesis is that it is the time needed for local collapses to propagate throughout the granular sample and to trigger the global liquefaction. This very short duration of null effective stress can help to explain the suddenness of the observed liquefaction phenomenon in nature.

In addition to the threshold void ratio e^{liq}_{30}, Fig. 23 gives the two other necessary conditions for liquefaction event inside the shaded rectangle: (a) the usual null effective isotropic stress ($\sigma' \approx 0$) and (b) the maintenance of this stress state (i.e. ΔU_{stable}) for at least 1 s above 95 % of ΔU_{stable} (or 5% of pore pressure dissipation). Collapse event can have a relatively longer duration for ΔU_{stable}, as indicated by large blue circle, and not terminate in a full liquefaction due to the presence of positive σ'.

It is worth mentioning some shared characteristics (damped transient oscillatory phase, short duration of pore pressure peak and distinct banging noise) of these spontaneous collapses in triaxial isotropic compression with the well-known century-old hydraulic shock of water hammer phenomenon in fluid mechanics. Nevertheless, many features of the transient phase are still the subject of hot debate among scientists, even today [31].

4.4 Dynamic consolidation

The first phase *I* of the dynamic time evolution of ΔU represents the very rapid oscillations in Fig. 9, which can be approximated by the standard equation (1) of vibrating systems [76]. Two generic parameters, damping factor ζ and

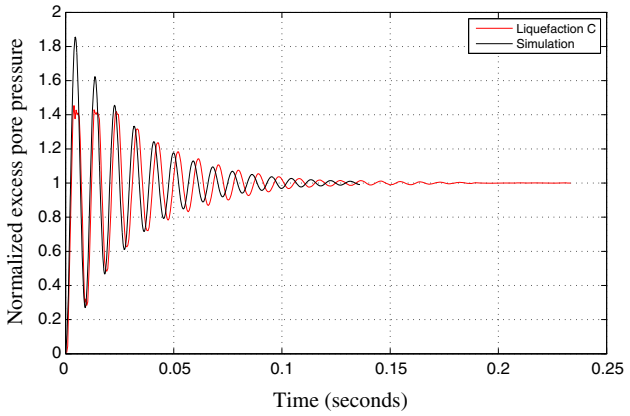

Fig. 24 Modelling of normalized transient behaviour of pore water pressure in liquefaction event of test I04 with $\zeta = 0.05$, $\omega_n = 693.5$

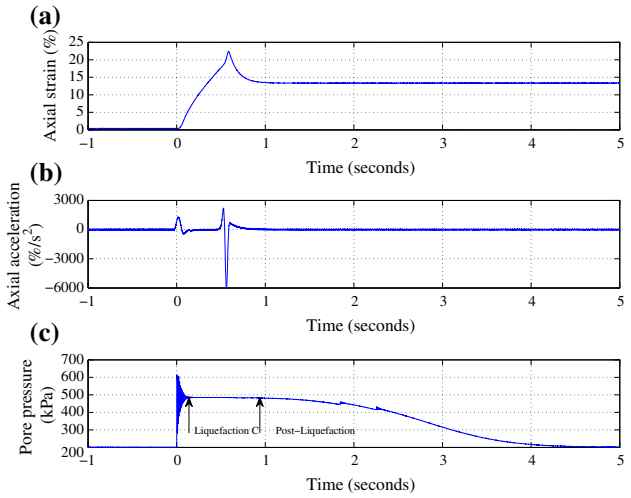

Fig. 25 Dynamic consolidation: axial strain (**a**), axial acceleration (**b**), excess pore pressure (**c**) of test I04

natural frequency ω_n, control this second-order equation:

$$\ddot{x} + 2\zeta\omega_n\dot{x} + \omega_n^2 x = 0 \tag{1}$$

For vibrating systems, ζ can be estimated using the logarithmic decrement, and ω_n the damped period. In our case, since all collapses have non constant logarithmic decrement in Fig. 11, ζ and ω_n are approximately identified by trial and error from the measurements of the first few peaks. Figure 24 shows a typical simulation of the normalized transient oscillatory behaviour of ΔU in liquefaction event C of test I04 with $\zeta = 0.05$ and $\omega_n = 693.5$. Reasonable results for a unit step load are obtained for an under-damped system, $0 < \zeta < 1$, especially for the first peaks. It means that the transient oscillatory behaviour of ΔU, or that of effective stress in a fully saturated system, in all liquefaction events is reasonably described by the normalized equation (1), independently of the isotropic triggering stress σ'_{trig} and of the stabilized ΔU_{stable}. However, while the numerical simulation presents a good comparison with pore pressure peaks, it predicts only 15 periods instead of 17 from experiment. Furthermore, the physical parameters of this simple spring-mass system cannot be derived and the subsequent phases *II* and *III* cannot be modeled by this equation.

Figure 25 shows a typical temporal evolution of excess pore pressure development including its full dissipation, together with axial strain and axial acceleration in a linear scale. The axial acceleration shows two pulses. The first pulse occurs at the beginning of the axial contraction with a time duration less than 200 ms. The coincidence of this pulse with the transient phase *I* strongly suggests the triggering of axial contraction by the fast pore pressure development. The second pulse concerns the peak of ε_a at constant effective stress state with no clear triggering source. Note that the two small aftershocks leave the axial strain state unchanged with a totally flat acceleration.

In the quest for a better understanding the liquefaction phenomenon, future studies will improve and explore further the dynamic measurements of axial and radial accelerations with miniaturized and submersible accelerometers inside the triaxial cell.

For an elastic media, the variation of pore pressure is related to the variation of volumetric strain [80]:

$$\Delta p = K\,\Delta\varepsilon_v \tag{2}$$

where K is the bulk modulus of the pore fluid. Considering the use of distilled water ($K = 2.25 \times 10^9 kg/ms^2$) in this project with fully saturated samples, a small change of volumetric strain in the order of 2.12×10^{-4} would suffice to raise the excess pore pressure to the maximal level of total stress of about 400 kPa in this study; hence annihilate the effective stress and and trigger the dangerous liquefaction. Consequently, it is possible, theoretically, to liquefy a pure elastic material under isotropic compression. However, in our knowledge, it has never been observed in soil laboratory, even for model granular materials. The logical and difficult question is: What could be the source capable of delivering this powerful pore pressure buildup?

4.5 Instability scenario

This isotropic liquefaction requires two basic ingredients: a loose density state and an initial structural anisotropic state. A fully saturated state and the perfectly spherical form of individual particle are two necessarily additional conditions. The first requirement of a loose density sample can be obtained artificially in laboratory using a common moist tamping and under compaction technique [7]. The second requirement can be the inherent anisotropic state of type II resulting from pre-

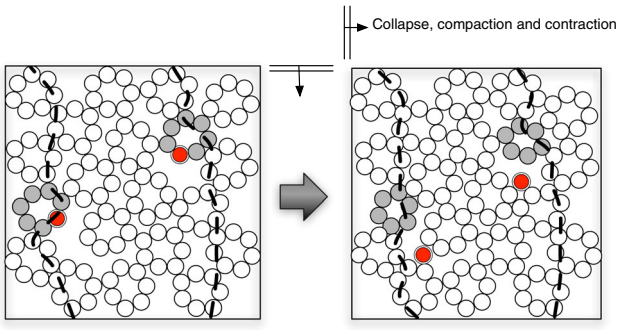

Fig. 26 Macropore hypothesis for loose model granular assembly (color figure online)

ferred orientation of unit vectors normal to contact surfaces of an assembly of spherical particles of model granular material [64].

Very loose glass bead samples created by moist tamping technique tend to have more irregular microstructures with the presence of macropores (large pores having the same size of aggregated grains), based on direct microscopic observations by Benahmed et al. [5] on Hostun sand using the same fabrication technique. This aggregated microstructures can qualitatively explain the tendency of loose samples to decrease in volume and the macropores are connected together through the force chains to support the applied stress. Figure 26 (left) shows a bidimensional conceptual scheme packing with identical macropores created with monodisperse disks.

It is well-known that the applied external forces were transmitted through the interparticle contact force network within a granular media [81], even from the early days of soil mechanics using photoelastic disk assemblies [23]. In the case of loose granular assemblies, it can be assumed that the force chains (thick dashed lines) pass through the connection points of macropores. Under external pressure, the force chains of such fragile structures can be broken, resulting in the ejection of one or more shaded red grains of the unstable honeycombed structures in Fig. 26 (right) prior to the collapse phase. The incompressibility of the pore water and the spherical grain shape facilitate probably the failures of already fragile contact chain forces and this ejection. The remaining grains still form a new macropore and the ejected grains in the fully saturated media transmit the ejecting force into the pore fluid, hence briefly raise the pore pressure to ΔU^{peak} and reduced later to ΔU^{stable}. Consequently, this very fast and strong buildup of ΔU reduces the effective mean pressure and accentuates the instability, without triggering it. Depending on the duration of ΔU^{stable}, therefore of the vanishing effective mean stress, the contact force network can fail or resume. The total failure of the contact force network means the total absence of particle contact under vanishing effective stress, resulting in cascading local failures propagating towards a global failure beyond repair and liquefaction can finally occur since the mixture of grains and water can flow like a fluid. The measured time duration needed to maintain a sufficient vanishing effective mean stress is of the order of seconds. The possibility of resuming and repairing the contact force network due to the progressive increase of σ' or dissipation of ΔU due to the drainage system indicates only a local failure and probably a new local rearrangement of the granular structures due to the incremental compaction [46]. The local or global failure of the contact network would explain the larger magnitudes of the collapse in saturated samples [19], compared to dry ones [1,3] in triaxial experiments; and the spontaneity of slip events in the experimental [30,62,73], or theoretical works [34].

It seems that extremely brief outbursts of pore water pressure can be associated with instabilities and failures of contact chain force, but exactly when and more importantly how and why they form are not yet known. In other words, the physical triggering mechanisms of these instabilities are still unknown. It is simply hypothesized that the ejection of spherical grains from the failure of contact force network has triggered the development of pore fluid pressure. It also suggests a sudden rearranging granular skeletons instead of gradually rearrangement.

Physical processes are needed to initiate the pore pressure buildup. The macropore hypothesis suggests a way in which failures of interparticle contact force network could be liquefaction seeds. We have asked whether the failures, with their accompanying propagations, are sufficient to boost the pore pressure development and cause a liquefaction.

Local collapses can be defined as dynamic instabilities not large enough, temporally and spatially, to propagate to the entire sample; and global collapse as dynamic instability able to sustain a vanishing effective stress state in sufficient time length resulting in an extremely weak contact force network causing catastrophic failure such as liquefaction.

This hypothesis of dynamic pore pressure fluctuations generating by sudden local rearrangements of granular microstructures capable of canceling the grain-contact stresses and propagating outward to the whole system with very large deformation in isotropic compression extends a step further the conjecture formulated earlier by Iverson and LaHusen [44] in rapid shearing experiments.

Modern μ-tomography technique [16,36], can be a candidate to follow in-situ the microstructure evolution leading to the collapse of such fragile structures, completely hidden from external visual observations, and possibly the physical mechanisms behind. However, this promising nondestructive approach has two inherent limitations linked to the loosely assemblies of idealized granular media: the temporal and the spatial resolution. The briefness of the dynamic instability phenomenon, below 5 ms, and the very short duration of the transient component, below 200 ms, cannot be fully captured

by the current tomography technique. The needed tracking of individual mono-size grain creates a new identification problem due to the monodispersivity of the used granular particles.

Recently, important progress has been made using very advanced equipments capable to track individual spherical grain in a polydisperse population [77]. It is known that structural rearrangement happens in very loose granular assemblies with a predominant role of particle rotation [79].

Advanced two or three-dimensional imaging techniques using epoxy impregnation [27,83], can also bring some post-mortem experimental supports for this microstructure evolution. Although capturing the dynamic collapse presents a great challenge, this destructive approach permits the quantification of macropores, before and after local and global catastrophic collapses, through the local pore size distribution, and can offer new useful insights.

Modern discrete element modeling technique can contribute to the understanding of these unconventional features. Recent advanced studies on a nearly monodispersed population of spherical grains, with a full solid–liquid coupling formulation, emphasizes the important role of pore fluid [32,33]. These numerical experiments indicate that model granular materials experience multiple liquefaction states, in the sense of vanishing effective stress, however very briefly within a few localized zones, in the order of 5 ms, even in drained compression. The idealized media quickly recover due to fast pore pressure dissipation. Unfortunately, no suitable indicator was found to when and where the next local collapse would occur. The dynamic characteristics of pore pressure evolution are still missing and remain currently a hot debate.

Recently, very sophisticated laser measurements suggest the accelerated creep as a possible indicator for advance instability warning in studying stick-slip phenomenon within well defined conditions inside a tribological laboratory [65], following the earlier suggestion [61]. The proposed equipments are currently beyond the normal capacity of most geotechnical laboratories.

Finally, note that in all these liquefaction experiments, no "doublet" (pair of beads joined by solid bridges) was found in binocular microscopy after testing, contrary to the stick-slip experiments in triaxial compression [19].

4.6 Repeatability and other materials

Despite a large number of tests on soda lime CVP glass beads, only 9 samples have liquefied out of more than 85 experiments. However, all tests presented dynamic instabilities. Although being rare, isotropic liquefaction has been repeatedly and consistently observed over more than two years of work experience with different experimentalists, and with two sizes of glass beads (SLG 2–4 and 6–8).

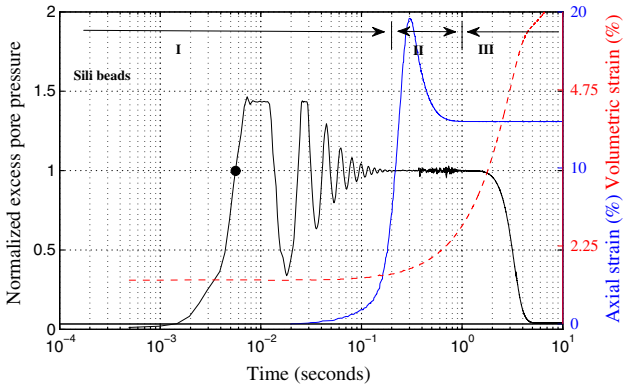

Fig. 27 Normalized behaviour of pore water pressure, axial strain and volumetric strain for liquefaction event at 496 kPa of test I10 on Sili beads type S

Spontaneous liquefaction has also been observed with other glass beads of different chemical composition and different industrial fabrication processes (Sili beads type S by Sigmund-Lindner.[2]) These beads have a more symmetrical distribution in size than CVP beads and centered on smaller mean diameter of 0.675 mm as shown in Fig. 1. They are also less rounded. The behaviour of normalized pore water pressure (although saturated), axial strain and volumetric strain for the only one observed liquefaction event at 496 kPa on Sili beads in Fig. 27 closely resembles the synthetic analysis in Fig. 22. This event has the largest magnitude of σ'_{trig}, without any preceding collapse or precursor.

The results of SLG 2-4 (black star) and Sili beads (green symbols) fulfill nicely the three necessary conditions for a full liquefaction: density state loose enough above the threshold void ratio e_{30}^{liq} in Fig. 20, and effective stress state small enough approaching the null value for at least 1 s in Fig. 23. The effects of σ'_{trig} on the measured macroscopic parameters follow the same evolutional trends in Figs. 18 and 22.

4.7 Liquefaction under drained triaxial compression

Another logical question arises: If the idealized and very loose granular assemblies survive the isotropic consolidation, can they experience the total liquefaction during the subsequent drained triaxial shearing in compression?

Figure 28 shows the isotropic consolidation experiencing one local collapse and without liquefaction for loose sample, $e_{30} = 0.675$, for test CID, up to 100 kPa, conformed to a liquefaction-free behaviour. However, Fig. 29 illustrates, once again, the unusual drained behaviour of model granular materials in triaxial compression with only one sudden slip accident associated with liquefaction at deviatoric level of 41 kPa and axial strain of only 0.0235 %. The mobilized

[2] www.Sigmund-Lindner.com.

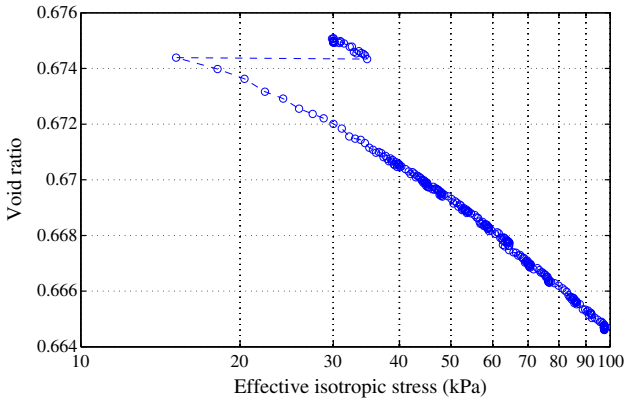

Fig. 28 Isotropic consolidation without liquefaction for loose sample above e_{30}^{liq} with $e_{30} = 0.675$ of drained compression test CID

friction angle of 9°8 at first slip occurrence is in the same order, although smaller, of that found in previous study on the same glass beads, albeit from a different batch [19].

Figure 30 gives the time evolution of axial strain, volumetric strain, deviatoric stress and excess pore pressure centering around the liquefaction phenomenon acquired by fast measurement system. This graphic conveys a false impression of déjà vu excepting a large deviatoric drop towards the null stress state during the first slip phase. The evolutional characteristics of pore pressure development, axial contraction and volumetric compaction of the slip phase under shear are very similar to those of spontaneous liquefaction under isotropic consolidation. Note particularly the large event in the post-liquefaction regime, associated with an additional volumetric compaction and axial extension before attaining the final constant axial strain state.

The ΔU^{norm} of the liquefaction event under drained shear is superimposed with dashed line in Fig. 22a with practically little visual difference. It means the isotropic instabilities and the slip phase of the stick-slip phenomenon share probably the same physical origin.

In previous works, the slip component of the stick-slip phenomenon is always associated with sudden deviatoric stress drop, axial strain jump, volumetric strain compaction, and from time to time sudden surge of ΔU, resulting in very high and narrow peak with fast dissipation. These characteristics are found again in Fig. 29 with a deviatoric drop to zero in only 3 ms, an exceptional large axial strain jump of nearly 14 % and a mild volumetric compaction of only 0.64 %. Furthermore, the very short-lived pore pressure peaks are captured in more details in this paper. More importantly, the newly performed experiments assess the dynamic characteristics of the slip phase and incidentally show the real possibility of total collapse by liquefaction during the slip phase in drained compression, due to the spontaneous and random development of ΔU. Together, these works point to the structural instability as a possible physical origin of the stick-slip phenomenon during shear and of the col-

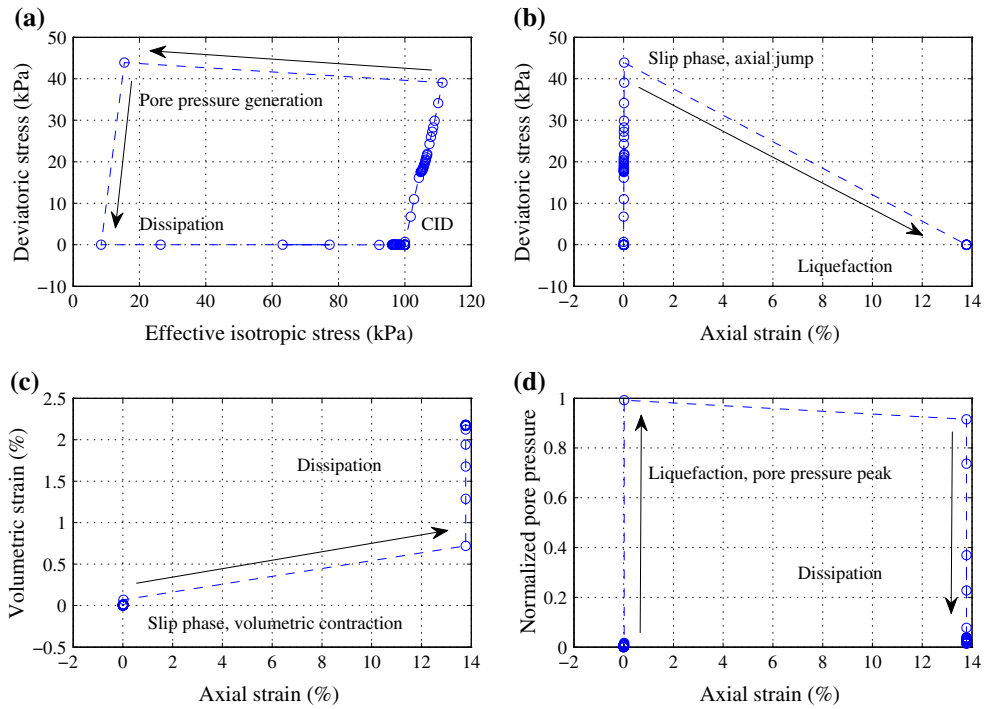

Fig. 29 Effective stress path (**a**), stress-strain behaviour (**b**), volumetric strain (**c**) and normalized excess pore pressure (**d**) of drained compression test CID

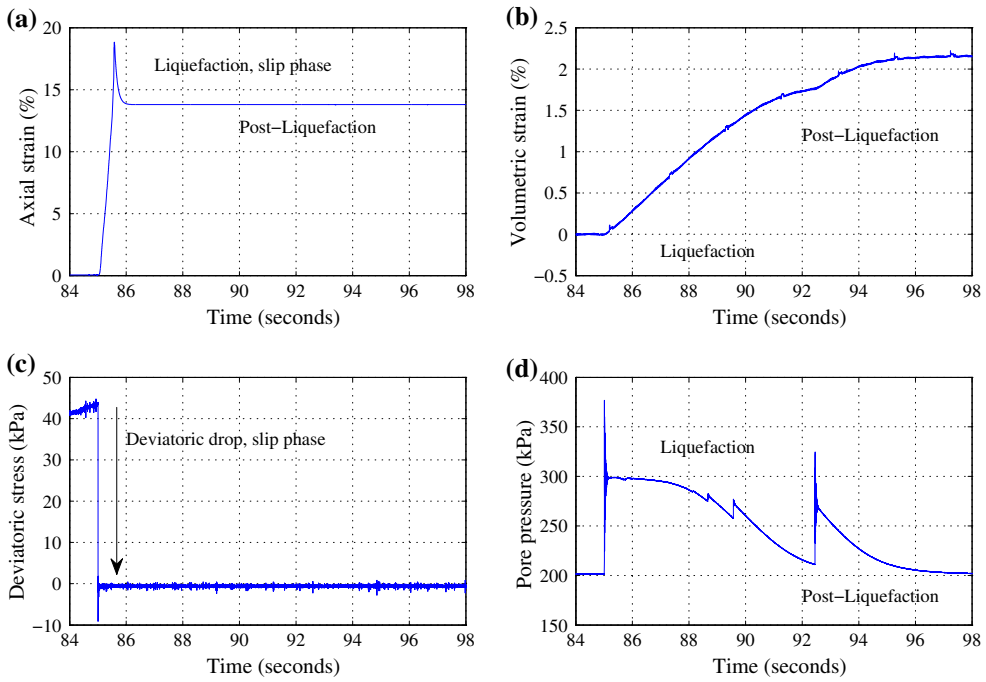

Fig. 30 Axial strain (**a**), volumetric strain (**b**), deviatoric stress (**c**) and excess pore pressure (**d**) as function of elapsed time since the start of drained compression test CID

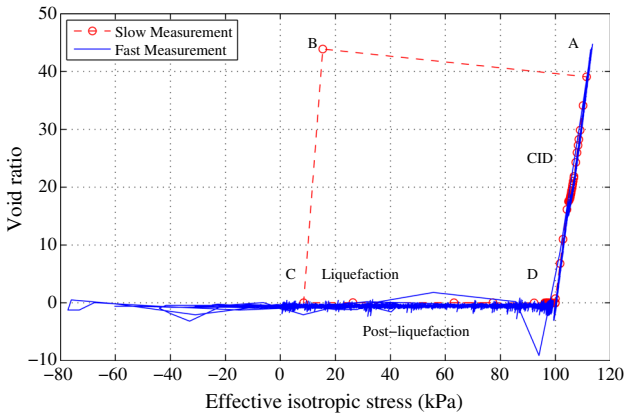

Fig. 31 True stress effective stress path (*blue line*) of test CID during the slip phase in triaxial drained compression (color figure online)

lapse, local or global, during isotropic consolidation. This test is the first known experimental evidence supporting the numerical simulation showing temporarily liquefaction in drained conditions for initially dense state, Goren et al. [33]. However, no transient phase was detected in the numerical experiment.

The slow data acquisition system gives an unrealistic frictional angle of 74°7 at pore pressure peak (hollow red point B and dashed line in Fig. 31), even briefly for only one measurement, since it is clearly situated outside the usual range of granular materials. The correct effective stress path in the slip phase, in continuous blue line, revealed by adequate acquisition system, continues to follow the classical straight line CID of drained compression down to point D, instead of point B, and moves subsequently toward the liquefaction state of point C, obliterating the next stick component.

One of the numerous questions raised by previous works [19], concerns the sudden pore pressure development : Could the unexpected surge of ΔU in the slip phase be strong enough to annihilate the total stress, and long enough to sustain the null effective stress state of liquefaction? This paper offers an obvious response, solving then at least one small mystery of model granular media.

5 Conclusions

This paper examines the possibilities offered by classical and versatile axisymmetric triaxial soil mechanic machines to explore an unknown aspect of the mechanical behaviour of idealized granular materials. It presents a detailed study of the isotropic consolidation behaviour of very loose and fully saturated monodisperse glass beads prepared by moist tamping technique. This paper provides the first full report of spontaneous liquefaction under *drained isotropic* compression of glass beads and reveals some mechanisms underlying the diffuse instability phenomenon, usually hidden or partially developed in sands.

Two basic ingredients are required to perform this unexpected isotropic liquefaction, a never observed before behaviour for real granular media: a loose density state and an initial

structural anisotropic state of monodispersed model granular material.

Each spontaneous isotropic liquefaction event occurring under undetermined isotropic stress can be characterised in three phases. The first short dynamic transient phase *I*, lasting less than 200 ms, has a very fast excess pore pressure development ΔU, vibrating like an oscillating underdamped system and creating a reduced stress state with null σ'. The second longer phase *II*, with sustainable state of vanishing σ' for at least 1 s, is responsible for creating a full liquefaction state with very large deformation. The last phase *III* permits the recover of σ' to the previous steady state before the liquefaction event. At least three necessary conditions should be fulfilled to have an instantaneous liquefaction: the granular assembly should be loose enough above the threshold void ratio e_{30}^{liq}, and the effective stress state small enough approaching the zero value for at least 1 s. The isotropic triaxial compression is liquefaction-free for loose state below e_{30}^{liq}.

These experimental observations greatly increase the complexity of modelling together the global and local behaviours of idealized granular materials. Nevertheless, this paper offers new experimental insights into the still mysterious spontaneous liquefaction under isotropic consolidation, even for model granular media. The unambiguous identification of the triggering mechanism of the collapse phenomenon, similar to the slip component of the stick-slip phenomenon, is still unknown. One of the possible driving mechanism can be the propagation of local subsequent failures of the force chains or the collapse of the unstable honeycombed macropores. The pore fluid is not the cause of the observed liquefaction. It merely amplifies the event due to the large duration of the stable phase *II* with sustainable null σ', responsible for the destruction of the granular micro-structure. However, current knowledge remains far from fully understanding how the instability of loosely bound and fully saturated granular assemblies works.

The questions asked in the introduction remain unanswered: What are the physical triggering mechanisms, leading to this powerful and instantaneous buildup of ΔU capable of annihilating σ' for a sufficient length of time to create catastrophic failures such as liquefaction or landslide? What are the physical parameters controlling this pore pressure evolution, especially in the transient oscillatory phase *I* and the crucial stable phase *II*? Our attempt to answer the above questions only adds a new layer to the intrigue.

Although isotropic liquefaction and stick-slip behaviour are still unknown to theoretical and numerical scientists, the experimental results of this paper may offer new clues to how granular liquefaction is formed. Despite many new difficult challenges to model the observed behaviour, several useful directions can be pointed out. New contact models integrating realistic rolling, sliding and torsion features of spherical particle may be introduced into DEM modelling [28]. Promising ideas in the quest for the triggering mechanisms can be explored and compared with the newly acquired experimental data of this paper within the field of constitutive modelling. To cite a few: the burst of kinetic energy leading to a dynamic regime [63], the sudden rearrangement of small number of grains [78], the localised reorganisations toward the progressive emergence of cooperative effects [55], the simple universal predictions based on mean field theory and event statistics [13], the elastic instability of Granular Solid Hydrodynamic theory [35] as well as the meso-scale model with local minimum density energy [49] or the fiber bundle model [60]. The test data as described here can be downloaded from the journal website as supplementary material.

Acknowledgments The authors would like to thank Dr. C. Dano of Ecole Centrale de Nantes, France for providing e_{min}, e_{max} and the SEM figures of glass beads for this study. Special thanks are also due to our colleagues, J. Scheibert and J.-N. Roux, for very fruitful discussions.

References

1. Adjemian, F., Evesque, P.: Experimental study of stick-slip behaviour. Int. J. Num. Anal. Meth. Geom. **28**(6), 501–530 (2004)
2. Agnolin, I., Roux, J.-N.: Internal states of model isotropic granular packings. II. Compression and pressure cycles. Phys. Rev. E **76**(6), 061303 (2007)
3. Alshibli, K.A., Roussel, L.E.: Experimental investigation of stick-slip behaviour in granular materials. Int. J. Num. Anal. Meth. Geom. **30**(14), 1391–1407 (2006)
4. Andreotti, B., Forterre, Y., Pouliquen, O.: Granular Media: Between Fluid and Solid. Cambridge University Press, Cambridge (2013)
5. Benahmed, N., Canou, J., Dupla, J.C.: Structure initiale et propriétés de liquéfaction statique d'un sable. Comptes Rendus Mécanique **332**(11), 887–894 (2004)
6. Biswas, B., Ray, P., Chakrabarti, B.K.: Statistical Physics of Fracture, Breakdown and Earthquake. Wiley, New Jersey (2015)
7. Bjerrum, L., Krimgstad, S., Kummeneje, O.: The shear strength of a fine sand. In: Proceedings of 5th International Conference on Soil Mechanics andFoundation Engineering, vol. 1, pp 29–37 (1961)
8. Bourne, N.: Materials in Mechanical Extremes. Cambridge University Press, Cambridge (2013)
9. Çabalar, A.F., Clayton, C.R.I.: Some observations of the effects of pore fluids on the triaxial behaviour of a sand. Granul. Matter **12**(1), 87–95 (2010)
10. Cambou, B., Nouguier-Lehon, C., Dubujet, Ph: Anisotropy in granular materials at different scales. Mech. Mater. **36**(12), 1185–1194 (2004)
11. Casagrande, A.: Liquefaction and Cyclic Deformation of Sands: A Critical Review. Harvard soil mechanics series. Harvard University, Cambridge (1975)
12. Castro, G.: Liquefaction of Sands. Harvard University, Cambridge, Harvard soil mechanics series (1969)
13. Dahmen, K.A., Ben-Zion, Y., Uhl, J.T.: Micromechanical model for deformation in solids with universal predictions for stress-strain curves and slip avalanches. Phys. Rev. Lett. **102**, 175501 (2009)
14. Daouadji, A., Darve, F., Al Gali, H., Hicher, P.Y., Laouafa, F., Lignon, S., Nicot, F., Nova, R., Pinheiro, M., Prunier, F., Sibille, L., Wan, R.: Diffuse failure in geomaterials: experiments, theory

and modelling. Int. J. Num. Anal. Meth. Geom. **35**(16), 1731–1773 (2011)
15. De Alba, P.A., Seed, H.B., Chan, C.K.: Sand liquefaction in large-scale simple shear tests. J. Geotech. Eng. ASCE **102**(9), 909–927 (1976)
16. Desrues, J., Chambon, R., Mokni, M., Mazerolle, F.: Void ratio evolution inside shear bands in triaxial sand specimens studied by computed tomography. Géotechnique **46**(3), 527–546 (1996)
17. Doanh, T., Dubujet, Ph, Protière, X.: On the undrained strain induced anisotropy of loose sand. Acta Geotechnica **8**(3), 293–309 (2013)
18. Doanh, T., Dubujet, Ph, Touron, T.: Exploring the undrained induced anisotropy of Hostun RF loose sand. Acta Geotechnica **5**(4), 239–256 (2010)
19. Doanh, T., Hoang, M.T., Roux, J.-N., Dequeker, C.: Stick-slip behaviour of model granular materials in drained triaxial compression. Granul. Matter **15**(1), 1–23 (2013)
20. Doanh, T., Ibraim, E.: Minimum undrained strength of Hostun RF. Géotechnique **50**(4), 377–392 (2000)
21. Doanh, T., Ibraim, E., Matiotti, R.: Undrained instability of very loose Hostun sand in triaxial compression and extension. Part 1: Experimental observations. Mech. Cohesive-Friction. Mater. **2**(1), 47–70 (1997)
22. Doanh, T., Le Bot, A., Abdelmoula, N., Hans, S., Boutin, C.: Liquefaction of immersed granular media under isotropic compression. Europhys. Lett. **108**(2), 24004 (2014)
23. Drescher, A., De Josselin de Jong, G.: Photoelastic verification of a mechanical model for the flow of a granular material. J. Mech. Phys. Solids **20**, 337–351 (1972)
24. Finge, Z., Doanh, T., Dubujet, Ph: Undrained anisotropy of Hostun RF loose sand : New experimental hints. Can. Geotech. J. **43**(11), 1195–1212 (2006)
25. Flavigny, E., Desrues, J., Palayer, B.Le: sable Hostun RF. Revue Française de Géotechnique **53**, 67–69 (1990)
26. Fragaszy, R., Voss, M.: Undrained compression behavior of sand. J. Geotech. Eng. ASCE **112**(3), 334347 (1986)
27. Frost, J.D., Jang, D.J.: Evolution of sand microstructure during shear. J. Geotech. Geoenviron. Eng. **126**(2), 116–130 (2000)
28. Fuchs, R., Weinhart, T., Meyer, J., Zhuang, H., Staedler, T., Jiang, X., Luding, S.: Rolling, sliding and torsion of micron-sized silica particles: experimental, numerical and theoretical analysis. Granul. Matter **16**(3), 281–297 (2014)
29. Gajo, A., Piffer, L.: The effects of preloading history on the undrained behaviour of saturated loose sand. Soils Found. **39**(6), 43–54 (1999)
30. Géminard, J.C., Losert, W., Gollub, J.P.: Frictional mechanics of wet granular material. Phys. Rev. E **59**(5), 5881–5890 (1999)
31. Ghidaoui, M.S., Zhao, M., McInnis, D.A., Axworthy, D.H.: A review of water hammer theory and practice. Appl. Mech. Rev. **58**(1), 49–76 (2005)
32. Goren, L., Aharonov, E., Sparks, D., Toussaint, R.: Pore pressure evolution in deforming granular material: a general formulation and the infinitely stiff approximation. J. Geophys. Res. **115**, B09216 (2010). doi:10.1029/2009JB007191
33. Goren, L., Aharonov, E., Sparks, D., Toussaint, R.: The mechanical coupling of fluid-filled granular material under shear. Pure Appl. Geophys. **168**(12), 2289–2323 (2011)
34. Griffa, M., Ferdowsi, B., Guyer, R.A., Daub, E.G., Johnson, P.A., Marone, C., Carmeliet, J.: Influence of vibration amplitude on dynamic triggering of slip in sheared granular layers. Phys. Rev. E **87**(1), 012205 (2013)
35. Gudehus, G., Jiang, Y., Liu, M.: Seismo- and thermodynamics of granular solids. Granul. Matter **13**(4), 319–340 (2011)
36. Hall, S.A., Bornert, M., Desrues, J., Pannier, Y., Lenoir, N., Viggiani, G., Bésuelle, P.: Discrete and continuum analysis of localised deformation in sand using X-ray μCT and volumetric digital image correlation. Géotechnique **60**(5), 315–322 (2010)
37. Hareb, H., Doanh, T.: Probing into the strain induced anisotropy of Hostun RF loose sand. Granul. Matter **14**(5), 589–605 (2012)
38. Igra, O., Seiler, F.: Experimental Methods of Shock Wave Research. Springer, New York (2016)
39. Ishihara, K.: Soil Behaviour in Earthquake Geotechnics. Oxford University Press, Oxford (1996)
40. Ishihara, K., Li, S.: Liquefaction of saturated sand in triaxial torsion shear test. Soils Found. **12**(1), 19–39 (1972)
41. Ishihara, K., Okada, S.: Undrained deformation and liquefaction of sand under cyclic stresses. Soils Found. **15**(1), 29–44 (1975)
42. Ishihara, K., Okada, S.: Yielding of overconsolidated sand and liquefaction model under cyclic stresses. Soils Found. **18**(1), 57–72 (1978)
43. Ishihara, K., Okada, S.: Effects of large preshearing on cyclic behaviour of sand. Soils Found. **22**(3), 109–125 (1982)
44. Iverson, R.M., LaHusen, R.G.: Dynamic pore-pressure fluctuations in rapidly shearing granular materials. Science **246**(4931), 796–799 (1989)
45. Jefferies, M., Been, K.: Soil Liquefaction. Taylor & Francis, New York (2006)
46. Kabla, A., Debrégeas, G.: Contact dynamics in a gently vibrated granular pile. Phys. Rev. Lett. **92**(3), 035501 (2004)
47. Konrad, J.M., Flavigny, E., Megachou, M.: Comportement non drainé du sable d'Hostun lâche. Revue Française de Géotechnique **54**, 53–63 (1991)
48. Krehl, P.: History of Shock Waves, Explosions and Impact. Springer, New York (2009)
49. Kumar, N., Luding, S.: Memory of jamming—multiscale models for soft and granular matter. Granul. Matter (2016, in press). arXiv:1407.6167
50. Ladd, R.S.: Preparing test specimens using undercompaction. Geotech. Test. J. **1**(1), 16–23 (1978)
51. Lade, P.V., Duncan, J.M.: Cubical triaxial tests on cohesionless soil. J. Soil Mech. Found. ASCE **99**(10), 793–812 (1973)
52. Lade, P.V., Nelson, R.B., Ito, Y.M.: Instability of granular materials with nonassociated flow. J. Eng. Mech. ASCE **114**(12), 2173–2191 (1988)
53. Lade, P.V., Yamamuro, J.A.: Physics and Mechanics of Soil Liquefaction. Balkema, Rotterdam (1999)
54. Lanier, J., Di Prisco, C., Nova, R.: Etude expérimentale et analyse théorique de l'anisotropie induite du sable Hostun. Revue Française de Géotechnique **57**, 59–74 (1993)
55. Le Bouil, A., Amon, A., McNamara, S., Crassous, J.: Emergence of cooperativity in plasticity of soft glassy materials. Phys. Rev. Lett. **112**, 246001 (2014)
56. Majmudar, T.S., Behringer, R.P.: Contact force measurements and stress-induced anisotropy in granular materials. Nature **435**, 1079–1082 (2005)
57. Masuda, T., Tatsuoka, F., Yamada, S., Sato, T.: Stress-strain behavior of sand in plane strain compression, extension and cyclic loading tests. Soils Found. **39**(5), 31–45 (1999)
58. Mašín, D.: Asymptotic behaviour of granular materials. Granul. Matter **14**(6), 759–774 (2012)
59. McDowell, G.R., Bolton, M.D.: A micro mechanical model for isotropic cyclic loading of isotropically clastically compressed soil. Granul. Matter **1**(4), 183–193 (1999)
60. Michlmayr, G., Or, D.: Mechanisms for acoustic emissions generation during granular shearing. Granul. Matter **16**(5), 627–640 (2014)
61. Nasuno, S., Kudrolli, A., Bak, A., Gollub, J.P.: Time-resolved studies of stick-slip friction in sheared granular layers. Phys. Rev. E **58**(2), 2161–2171 (1998)
62. Nasuno, S., Kudrolli, A., Gollub, J.P.: Friction in granular layers: hysteresis and precursors. Phys. Rev. Lett. **79**(5), 949–952 (1997)

63. Nicot, F., Daouadji, A., Laouafa, F., Darve, F.: Second-order work, kinetic energy and diffuse failure in granular materials. Granul. Matter **13**(1), 19–28 (2011)
64. Oda, M., Iwashita, K.: Mechanics of Granular Materials: An Introduction. CRC Press, boca raton (1999)
65. Popov, V.L., Grzemba, B., Starcevic, J., Fabry, C.: Accelerated creep as a precursor of friction instability and earthquake prediction. Phys. Mesomech. **13**(5–6), 283–291 (2010)
66. Ramos, A.M., Andrade, J.E., Lizcano, A.: Modelling diffuse instabilities in sands under drained conditions. Géotechnique **62**(4), 471–478 (2012)
67. Schofield, A., Wroth, P.: Critical State Soil Mechanics. McGraw-Hill, New York (1968)
68. Seed, H.B., Lee, K.L.: Liquefaction of saturated sands during cyclic loading. J. Soil Mech. Found. ASCE **92**(6), 105–134 (1966)
69. Sitharam, T.G., Vinod, J.S.: Critical state behaviour of granular materials from isotropic and rebounded paths: DEM simulations. Granular Matter **11**(1), 33–42 (2009)
70. Stavropoulou, M.: A model of liquefaction of granular materials in isotropic compression. Eur. J. Environ. Civil Eng. **14**(8–9), 1113–1128 (2010)
71. Terzaghi, K., Peck, R.P., Mesri, G.: Soil Mechanics in Engineering Practice, 3rd edn. Wiley, New Jersey (1996)
72. Towhata, I.: Geotechnical Earthquake Engineering. Springer, New York (2008)
73. Tsai, J.-C., Voth, G.A., Gollub, J.P.: Internal granular dynamics, shear-induced crystallization, and compaction steps. Phys. Rev. Lett. **91**(6), 064301 (2003)
74. Vaid, Y.P., Chung, E.K.F., Kuerbis, R.H.: Preshearing and undrained response of sands. Soils Found. **29**(4), 49–61 (1989)
75. Verdugo, R., Ishihara, K.: The steady state of sandy soils. Soils Found. **36**(2), 81–91 (1996)
76. Verruijt, A.: An Introduction to Soil Dynamics. Springer, New York (2010)
77. Vlahinić, I., Andò, E., Viggiani, G., Andrade, J.: Towards a more accurate characterization of granular media: extracting quantitative descriptors from tomographic images. Granul. Matter **16**(1), 9–21 (2014)
78. Welker, P., McNamara, S.: Precursors of failure and weakening in a biaxial test. Granul. Matter **13**(1), 93–105 (2011)
79. Wenzl, J., Seto, R., Roth, M., Butt, H.-J., Auernhammer, G.K.: Measurement of rotation of individual spherical particles in cohesive granulates. Granul. Matter **15**(4), 391–400 (2013)
80. Wood, D.M.: Soil Behaviour and Critical State Soil Mechanics. Cambridge University Press, Cambridge (1990)
81. Wood, D.M., Lesniewska, D.: Stresses in granular materials. Granul. Matter **13**(4), 395–415 (2011)
82. Yamada, S., Takamori, T., Sato, K.: Effects on reliquefaction resistance produced by changes in anisotropy during liquefaction. Soils Found. **50**(1), 9–25 (2010)
83. Yang, X.: *Three-dimensional Characterization of Inherent and Induced Sand Microstructure*. Phd thesis, Georgia Institute of Technology, (2005)
84. Yoshimi, Y., Tokimatsu, K., Kaneko, O., Makihara, Y.: Undrained cyclic shear strength of a Niigata sand. Soils Found. **24**(4), 131–145 (1984)